Title

Intrabronchial Infection of Rhesus Macaques with Simian Varicella Virus Results in a Robust Immune Response in the Lungs

Journal

Journal of Virology, 88(21)

ISSN

0022-538X

Authors

Haberthur, Kristen
Meyer, Christine
Arnold, Nicole
et al.

Publication Date

2014-11-01

DOI

10.1128/jvi.01814-14

Peer reviewed

JVI Journals.ASM.org

Intrabronchial Infection of Rhesus Macaques with Simian Varicella Virus Results in a Robust Immune Response in the Lungs

Kristen Haberthur,[a] Christine Meyer,[b] Nicole Arnold,[c] Flora Engelmann,[d] Daniel R. Jeske,[e] Ilhem Messaoudi[b,c,d]

Graduate Program in Molecular Microbiology and Immunology, Oregon Health and Science University, Portland, Oregon, USA[a]; Division of Pathobiology and Immunology, Oregon National Primate Research Center, Beaverton, Oregon, USA[b]; Graduate Program in Microbiology, University of California Riverside, Riverside, California, USA[c]; Division of Biomedical Sciences, School of Medicine, University of California Riverside, Riverside, California, USA[d]; Department of Statistics, University of California Riverside, Riverside, California, USA[e]

ABSTRACT

Varicella-zoster virus (VZV) is the etiological agent of varicella (chickenpox) and herpes zoster (shingles). Primary VZV infection is believed to occur via the inhalation of virus either in respiratory droplets or from shedding varicella lesions or by direct contact with infectious vesicular fluid. However, the ensuing immune response in the lungs remains incompletely understood. We have shown that intrabronchial inoculation of rhesus macaques with simian varicella virus (SVV), a homolog of VZV, recapitulates the hallmarks of acute and latent VZV infection in humans. In this study, we performed an in-depth analysis of the host immune response to acute SVV infection in the lungs and peripheral blood. We report that acute SVV infection results in a robust innate immune response in the lungs, characterized by the production of inflammatory cytokines, chemokines, and growth factors as well as an increased frequency of plasmacytoid dendritic cells (DCs) that corresponded with alpha interferon (IFN-α) production and a rapid decrease in viral loads in the lungs. This is followed by T and B cell proliferation, antibody production, T cell differentiation, and cytokine production, which correlate with the complete cessation of viral replication. Although terminally differentiated CD8 T cells became the predominant T cell population in bronchoalveolar lavage cells, a higher percentage of CD4 T cells were SVV specific, which suggests a critical role for these cells in the resolution of primary SVV infection in the lungs. Given the homology between SVV and VZV, our data provide insight into the immune response to VZV within the lung.

IMPORTANCE

Although primary VZV infection occurs primarily via the respiratory route, the host response in the lungs and its contribution to the cessation of viral replication and establishment of latency remain poorly understood. The difficulty in accessing lung tissue and washes from individuals infected with VZV has hampered efforts to address this knowledge gap. SVV infection of rhesus macaques is an important model of VZV infection of humans; therefore, we utilized this animal model to gain a comprehensive view of the kinetics of the immune response to SVV in the lung and its relationship to the resolution of acute infection in respiratory tissues. These data not only advance our understanding of host immunity to VZV, a critical step in developing new vaccines, but also provide additional insight into immunity to respiratory pathogens.

Primary infection with varicella-zoster virus (VZV), a neurotropic alphaherpesvirus, occurs primarily through the inhalation of virus-laden saliva droplets (1, 2) or airborne virions from varicella lesions (3) or by contact with infectious vesicular fluid (4). The incubation period of varicella can range from 10 to 21 days and usually results in a benign self-limiting disease characterized by the appearance of vesicular exanthem, fever, and malaise (5). Current evidence suggests VZV can infect and replicate within the respiratory mucosal epithelium. Indeed, VZV pneumonia is the most common complication of primary VZV infection in adults, where active viral replication occurs in the epithelial cells that line the pulmonary alveoli (6–8). Moreover, although VZV pneumonia is a rare complication of primary VZV infection in immunocompetent children (~1% varicella cases), it increases to ~50% in immunocompromised children, where it can be associated with high morbidity and sometimes mortality (9).

VZV infection of the respiratory mucosal epithelium is followed by infection of or capture by dendritic cells (DCs), which traffic to regional lymph nodes or tonsils and transfer VZV to T cells (10–12). Infected T cells then home to the skin to infect cutaneous epithelial cells, resulting in the characteristic varicella lesions (13–15). *In vitro* and *in vivo* studies using the humanized SCID mouse model have also demonstrated that tonsillar T cells are susceptible to VZV infection and can transport VZV to the skin (12, 13, 16). Clinical observations indicate that successful control of VZV is dependent on cellular rather than humoral immunity (17–20). However, the immune response to acute VZV infection in the respiratory tract remains incompletely defined.

Simian varicella virus (SVV) is a primate alphaherpesvirus that causes a varicella-like disease in macaques (21) and shares significant DNA homology with VZV (22–24). Given that the major route of primary VZV infection is via the respiratory tract, we developed a rhesus macaque model where animals are infected intrabronchially with SVV. This model results in a disease that

Received 20 June 2014 **Accepted** 18 August 2014
Published ahead of print 20 August 2014
Editor: L. M. Hutt-Fletcher
Address correspondence to Ilhem Messaoudi, messaoud@ucr.edu.
K.H. and C.M. contributed equally to this work.

doi:10.1128/JVI.01814-14

recapitulates the hallmarks of human varicella: (i) detectable viral DNA in both whole blood and bronchoalveolar lavage (BAL) cells, (ii) development of varicella-like clinical symptoms, (iii) development of innate and adaptive immune response, and (iv) establishment of latency with limited viral transcription in sensory ganglia (25, 26). The intrabronchial inoculation route results in a shorter incubation period than that of human varicella (7 to 10 instead of 14 to 21 days) but ensures a consistent disease phenotype in all inoculated animals.

In this study, we conducted a comprehensive analysis of the anti-SVV immune response in both the lungs as well as the peripheral blood following primary SVV infection of young rhesus macaques. Of importance, acute SVV infection in the lungs induces a strong innate immune response that includes an increase in the frequency of plasmacytoid DCs and a corresponding increase in alpha interferon (IFN-α) concentrations in the bronchoalveolar lavage (BAL) supernatant, which correlates with significant reduction in viral loads. Innate immune activation is then followed by an adaptive immune response that is characterized by the increased frequency of CD8 effector memory T cells and a robust SVV-specific CD4 T cell response. The data presented here expand our understanding of both the innate and adaptive host immune response to acute SVV infection in the lungs and improves our general understanding of immunity to respiratory pathogens in an important model of human disease.

MATERIALS AND METHODS

Ethics statement. This study was carried out in strict accordance with the recommendations described in the *Guide for the Care and Use of Laboratory Animals* (27) of the National Institutes of Health, the Office of Animal Welfare, and the United States Department of Agriculture. All animal work was approved by the Oregon National Primate Research Center Institutional Animal Care and Use Committee. All procedures were carried out under ketamine anesthesia in the presence of veterinary staff, and all efforts were made to minimize animal suffering.

Animals and sample collection. Sixteen colony-bred Indian-origin rhesus macaques (*Macaca mulatta*), 3 to 4 years of age (6 females and 10 males), were inoculated intrabronchially with 4×10^5 PFU wild-type simian varicella virus (SVV) as previously described (25). All animals were seronegative prior to inoculation. Whole blood (WB) and bronchoalveolar lavage (BAL) samples were collected from all 16 animals on days 0, 7, 14, 21, 28, 42, 56, 92, and 126 postinfection. In addition, WB and BAL samples were collected from 4 animals on days 3, 10, and 17. All samples were used in all the assays described below. BAL is performed by infusing three 10-ml aliquots of sterile pyrogen-free saline into the right and left lungs followed by aspiration using 120 mm of mercury absolute (mmHgA) of vacuum. On average, a total of 50 ml of BAL fluid was recovered from the lungs. BAL samples were pelleted and resuspended in RPMI 1640 medium (Thermo Scientific, Waltham, MA) supplemented with 10% fetal bovine serum (FBS) and streptomycin-penicillin and L-glutamine (PSG). Peripheral blood mononuclear cells (PBMC) and plasma were isolated by centrifugation over a density gradient cell separation medium (Corning, Manassas, VA) as per the manufacturer's recommendation and resuspended in RPMI with 10% FBS and PSG. The absolute number of neutrophils and lymphocytes within whole blood was obtained using a complete blood count machine (Hemavet; Drew Scientific Group, Waterbury, CT).

Cells and virus. Wild-type SVV was propagated in primary rhesus fibroblasts (RF) at 37°C in Dulbecco's modified Eagle's medium (DMEM) supplemented with 10% FBS and PSG. SVV-infected RF were cryopreserved in liquid nitrogen in FetalPlex (Gemini Bio Products, West Sacramento, CA) supplemented with 10% dimethyl sulfoxide (DMSO) and assayed by plaque assay. SVV cell lysate was obtained by collecting SVV-infected RF at the height of cytopathic effect (CPE) followed by sonication using 7 pulses of 70 to 80 W (Sonicator 3000; Misonix), centrifugation at 2,000 rpm for 5 min, and storage at −80°C.

DNA extraction and qPCR. DNA was extracted from whole blood and BAL cells using the ArchivePure DNA cell/tissue kit (5 PRIME, Gaithersburg, MD) according to the manufacturer's protocol. SVV DNA viral load was measured by quantitative real-time PCR (qPCR) using Maxima Probe/ROX qPCR master mix (2×) (Fermentas, Glen Burnie, MD) and primers/TaqMan probe specific for SVV open reading frame (ORF) 21, as previously described (25). Following an initial 10-min 95°C step, 40 cycles of 15 s at 95°C and 1 min at 60°C were completed using a StepOnePlus instrument (Life Technologies, Carlsbad, CA). SVV BAC DNA (28) was used as the quantification standard.

Complete blood analysis. White blood cell counts and differentials to determine lymphocyte and neutrophil percentages were obtained from whole blood using a complete blood count machine (Hemavet; Drew Scientific Group, Waterbury, CT). Percentages of cell subsets from flow cytometric analysis were converted to absolute numbers using the lymphocyte number per microliter of whole blood.

Identification of innate immune cell populations. PBMC and BAL cells were stained with antibodies against CD3 (BD Pharmingen, San Diego, CA), CD20 (Beckman Coulter, Brea, CA), CD14 (BioLegend, San Diego, CA), HLA-DR (BioLegend), CD11c (BioLegend), and CD123 (BioLegend) to delineate monocytes ($CD3^-$ $CD20^-$ $CD14^+$ $HLA\text{-}DR^+$) and dendritic cells (DCs; $CD3^-$ $CD20^-$ $CD14^-$ $HLA\text{-}DR^+$). DCs were further defined into myeloid (mDCs; $CD123^-$ $CD11c^+$) and plasmacytoid (pDCs; $CD123^+$ $CD11c^-$) DCs. Cells were fixed according to manufacturer recommendations (BioLegend) and analyzed using the LSRII instrument (Becton Dickenson, San Jose, CA) and FlowJo software (TreeStar, Ashland, OR).

Measurement of T and B cell proliferation. PBMC and BAL cells were surface stained with antibodies against CD8β (Beckman Coulter), CD4 (eBioscience, San Diego, CA), CD28 (BioLegend), CD95 (BioLegend), and CCR7 (BD Pharmingen), which allowed for the delineation of central memory (CM; $CD28^+$ $CD95^+$ $CCR7^+$), transitional effector memory (TEM; $CD28^+$ $CD95^+$ $CCR7^-$), and effector memory (EM; $CD28^-$ $CD95^+$ $CCR7^-$) CD4 and CD8 T cells. PBMC and BAL cells were also surface stained with antibodies against CD20, CD3, IgD (Southern Biotech, Birmingham AL), and CD27 (BioLegend) to delineate marginal zone-like (MZ-like; IgD^+ $CD27^+$), memory (IgD^- $CD27^+$), and double-negative (DN; IgD^- $CD27^-$) B cell subsets. Cells were fixed and permeabilized according to manufacturer recommendations (BioLegend) before the addition of a Ki67-specific antibody (BD Pharmingen). The samples were analyzed using the LSRII instrument and FlowJo software.

Granzyme B staining. PBMC and BAL cells were surface stained using antibodies against CD4, CD8β, CD28, CD95, and CCR7, as described above. Cells were fixed, permeabilized (BioLegend), and stained intracellularly using an antibody against granzyme B (BD Pharmingen). Samples were analyzed using the LSRII instrument and FlowJo software.

Intracellular cytokine staining (ICS). PBMC and BAL cells were stimulated *ex vivo* with SVV lysate (1 μg) or with an overlapping peptide pool representing ORFs 4, 11, 16, 31, and 37 (1 μg) for 1 h followed by the addition of brefeldin A (Sigma, St. Louis, MO) for an additional 14 h. We have recently shown that all 5 ORFs are highly immunogenic during acute SVV infection, and the cumulative response accounts for 20% of the total acute T cell response (29). After incubation, cells were stained with antibodies directed against CD4 and CD8β. Samples were fixed, permeabilized (BioLegend), and stained using antibodies against IFN-γ (eBioscience), tumor necrosis factor alpha (TNF-α) (eBioscience), macrophage inflammatory protein 1 beta (MIP-1β) (BD Pharmingen), or interleukin 2 (IL-2) (BioLegend). Samples were analyzed using the LSRII instrument and FlowJo software.

ELISA. Enzyme-linked immunosorbent assay (ELISA) plates were coated with SVV lysate overnight at 4°C, washed three times with 0.05% Tween-PBS, and incubated with heat-inactivated (56°C, 30 min) plasma

samples in 3-fold dilutions in triplicate for 1 h. After being washed three times with 0.05% Tween-PBS, horseradish peroxidase (HRP)-conjugated anti-rhesus IgG (Fitzgerald Industries, Acton, MA) or anti-rhesus IgM (Brookwood Biomedical, Birmingham, AL) was added for 1 h, followed by the addition of *o*-phenylenediamine·2HCl (OPD) substrate (Sigma). The reaction was stopped with the addition of 1 M HCl. IgG and IgM endpoint titers were calculated using log-log transformation of the linear portion of the curve and 0.1 optical density (OD) units at 490 nm as the cutoff. IgG titers were standardized using a positive-control sample that was included on every ELISA plate.

Cytokine analysis. BAL supernatant and plasma samples (stored at −80°C) were thawed and analyzed in duplicate using the Invitrogen cytokine monkey magnetic 28-plex panel (Life Technologies, Grand Island, NY), which includes monocyte chemoattractant protein 1 (MCP-1; CCL2), fibroblast growth factor basic (FGF-b), IL-1β, granulocyte colony-stimulating factor (G-CSF), IL-10, IL-6, IL-12, RANTES, eotaxin, IL-17, macrophage inflammatory protein 1 alpha (MIP-1α), granulocyte-macrophage colony-stimulating factor (GM-CSF), macrophage inflammatory protein 1 beta (MIP-1β), IL-15, epidermal growth factor (EGF), IL-5, hepatocyte growth factor (HGF), vascular endothelial growth factor (VEGF), IFN-γ, monocyte-derived chemokine (MDC; CCL22), interferon-inducible T cell alpha chemoattractant (ITAC; CXCL11), migration inhibition factor (MIF), IL-1 receptor agonist (IL-1RA), TNF-α, IL-2, monokine induced by IFN gamma (MIG; CXCL9), IL-4, and IL-8, and the cynomolgus/rhesus IFN-α ELISA kit according to the manufacturer's instructions (PBL Interferon Source, Piscataway, NJ).

Statistical analysis. Graphing was performed with GraphPad Prism software (GraphPad Software Inc., La Jolla, CA). (i) For viral loads in BAL and PBMC, one-way repeated-measures analysis of variance (ANOVA) with Dunnett's multiple comparison posttest was used to explore differences between days postinfection (dpi) and baseline (day 0) values. Viral loads were also compared using an area-under-curve (AUC) analysis. ANOVA was used to test if the mean AUC values were the same in the two locations after using a normal quantile plot to establish if the differences in the AUC values were approximately normally distributed. (ii) One-way repeated-measures ANOVA with Dunnett's multiple comparison posttest was used to explore differences in frequency of $Ki67^+$ cells between days postinfection and baseline (day 0) values. Peak times for the Ki67 immune response variables were identified by use of the repeated-measures model. Within-animal correlations were captured through a compound symmetric variance-covariance matrix for the error terms. Peaks in the Ki67 levels were identified through a Bonferroni-adjusted multiple comparison procedure of the least-squares means. (iii) ICS lysate and peptide response variables within BAL fluid and within PBMC were analyzed using a repeated-measures model with a compound symmetric variance-covariance structure. Significance values of T cell cytokine production utilized one-way repeated-measures ANOVA with Dunnett's multiple comparison posttest to explore differences between days postinfection and baseline (day 0) values. An overall F-test was used to test the hypothesis of no trend in the response, and a Dunnett-Hsu adjusted multiple comparison procedure was used to examine contrasts of the lowest available dpi level with all higher dpi levels. AUC analyses were used to compare overall levels of ICS lysate and ICS peptide variables. A total of 38 contrasts were made within BAL, within PBMC, and between BAL and PBMC. Contrasts were tested using a paired Wilcoxon signed-rank test due to the frequent violations of the normality assumption. The 38 contrasts were divided into four natural families, and individual Bonferroni multiple comparison-adjusted *P* values were used within each family. Differences in immune response levels (proliferation, T cell cytokine production) between BAL and PBMC were compared using a repeated-measures model for the within-animal difference. (iv) Antibody levels were analyzed using a left-censored Weibull regression to account for the lower detection limit threshold of 200 in plasma. Contrasts of the lowest available days postinfection (dpi) level with all higher dpi levels were tested using asymptotic chi-square tests from the fitted Weibull regression model.

RESULTS

SVV infection results in neutrophil and T cell recruitment into the lungs. Rhesus macaques ($n = 16$) 3 to 4 years of age were infected intrabronchially with 4×10^5 PFU wild-type simian varicella virus (SVV). All RMs displayed hallmarks of SVV varicella. SVV viral loads were measured in whole blood (WB) and bronchial alveolar lavage (BAL) samples by quantitative real-time PCR (qPCR). Viral loads in WB were detected by 3 days postinfection (dpi), peaked at 7 dpi ($P < 0.001$), and resolved below our limit of detection by approximately 14 dpi (Fig. 1A). In BAL cells, SVV viral loads increased significantly at 3 and 7 dpi compared to baseline ($P < 0.001$) before progressively declining to below our limit of detection by 42 dpi (Fig. 1A). Viral loads were substantially higher in BAL cells, the site of inoculation, than in WB (area under the curve [AUC] *P* value of <0.001).

To characterize the immune response to SVV, we assessed changes in the numbers of two major white blood cell populations, neutrophils and lymphocytes, following acute SVV infection in BAL cells and PBMC. The absolute cell count in BAL samples is reported from the total volume, 50 ml, recovered during the bronchoalveolar lavage procedure (Fig. 1B). The number of neutrophils in BAL supernatant increased on day 7, peaked at 10 dpi ($P < 0.05$), and returned to baseline levels by 21 dpi. Lymphocyte numbers in BAL supernatant also peaked at 10 dpi ($P < 0.01$) and returned to basal levels by 56 dpi (Fig. 1B). In peripheral blood, lymphocyte and neutrophil numbers fluctuated throughout the infection (Fig. 1C). Both cell populations initially decreased between 7 and 10 dpi, which was followed by an increase in cell counts between 14 and 21 dpi. Lymphocyte numbers in whole blood continued to decline from 14 dpi and returned to baseline levels by 92 dpi, while neutrophil counts decreased again at 56 dpi and returned to baseline by 92 dpi. To better understand SVV-induced changes in lymphocyte populations in the lungs, we measured the frequency of B and T cells using flow cytometry. CD20 B cells are rare in BAL samples, and their frequency did not significantly change during acute infection (Fig. 1D). The frequency of CD4 T cells also remained relatively stable throughout the study (Fig. 1D). In contrast, the relative frequency of CD8 T cells increased significantly at 10 dpi, peaked at 17 dpi ($P < 0.0001$), and remained the dominant lymphocyte population in BAL samples until 126 dpi (Fig. 1D). In PBMC, the frequency of CD20 B cells decreased at 3 dpi ($P < 0.0001$), remained lower than baseline until 14 dpi, and then returned to baseline levels (Fig. 1E). No significant changes were observed in either the CD4 or CD8 T cell population throughout the study (Fig. 1E).

Acute SVV infection results in increased chemokine, cytokine, and growth factor levels in the lungs. Given the changes in immune cell infiltration into the bronchoalveolar space following SVV infection, we measured the concentration of multiple chemokines, cytokines, and growth factors in BAL supernatant and plasma by multiplex Luminex technology (Fig. 2). In BAL fluid, concentrations of IL-4, IL-5, IL-8, IL-10, IL-17, granulocyte colony-stimulating factor (G-CSF), and granulocyte macrophage colony-stimulating factor (GM-CSF) were below our level of detection (data not shown). In contrast, acute SVV infection induced the expression of several chemokines (Fig. 2A). Levels of the chemokines MCP-1 (CCL2), MIP-1α (CCL3), and MIP-1β (CCL4), which are involved in recruiting monocytes, memory T cells, and DCs to sites of inflammation (30, 31), increased signif-

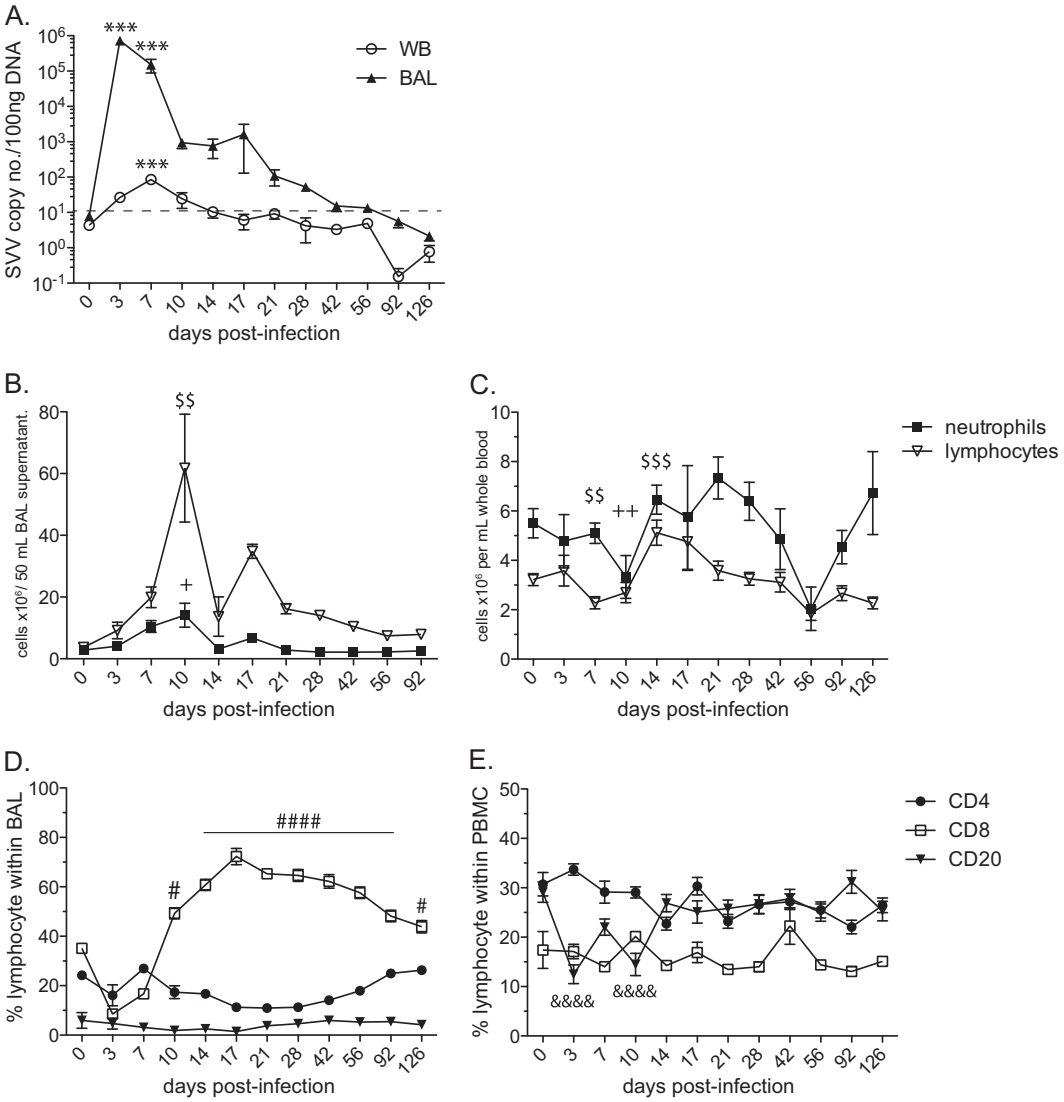

FIG 1 SVV infection results in changes in immune cell populations in the lungs. (A) Viral loads from BAL and WB samples were measured by qPCR using primers and probes specific for SVV ORF 21 and are shown as average copy numbers per 100 ng of DNA (***, $P < 0.001$). Dashed line indicates limit of detection. The absolute numbers (means ± standard errors of the means [SEM]) of neutrophils and lymphocytes were quantified from BAL supernatant per 50 ml (B) and WB per 1 ml (C) ($$, $P < 0.01$; $$$, $P < 0.001$ for lymphocytes (+, $P < 0.05$; ++, $P < 0.01$ for neutrophils). The frequencies of CD4 T, CD8 T, and CD20 B cells (means ± SEM) were determined in BAL samples (D) and PBMC (E) by flow cytometry (#, $P < 0.05$; ####, $P < 0.0001$ for CD8 T cells) (&&&&, $P < 0.0001$ for CD20 B cells).

icantly at 7 dpi ($P < 0.001$) and returned to basal levels by 14 dpi. Eotaxin, a chemotactic factor for eosinophils, basophils, and T helper type-2 (Th2) lymphocytes (32–34), was also significantly increased at 7 dpi ($P < 0.001$) and returned to basal levels by 14 dpi. MDC (CCL22), which is important for the recruitment of monocytes, DCs, and NK cells (35), remained significantly increased between 7 and 14 dpi ($P < 0.001$) before returning to baseline levels. MIG (CXCL9), a T cell chemoattractant induced by IFN-γ (36), and I-TAC (CXCL11), chemotactic for activated T cells (37), were detected at 7 dpi ($P < 0.001$). In contrast, levels of RANTES (CCL5), important for immune cell recruitment into inflammatory sites (38), increased at 21 dpi ($P < 0.001$), and levels remained significantly increased through 28 dpi ($P < 0.01$) in BAL fluid.

In addition to chemokines, SVV infection also induces the production of several cytokines (Fig. 2B). Levels of the inflammatory cytokines IL-1β (39), IL-6 (40), and TNF-α (41) were significantly increased over baseline at 7 dpi ($P < 0.001$). Moreover, two cytokines (among others) that play a role in T cell differentiation, namely, IL-15, which regulates the activation and proliferation of T cells and NK cells (42), and IL-12, which is important in the differentiation of naive T cells into CD4 helper type 1 T (Th1) cells (43), were significantly induced at 7 dpi ($P < 0.001$) and 14 dpi ($P < 0.001$), respectively. Acute SVV infection also induced the expression of key T cell cytokines (Fig. 2C). Specifically, IFN-γ, which is critical to the antiviral immune response and differentiation of Th1 subsets (44), and IL-2, which is involved in T cell proliferation and homeostasis (45), significantly increased at 7 dpi ($P < 0.001$) in BAL fluid.

Negative regulators (Fig. 2D) of inflammation, including IL-1

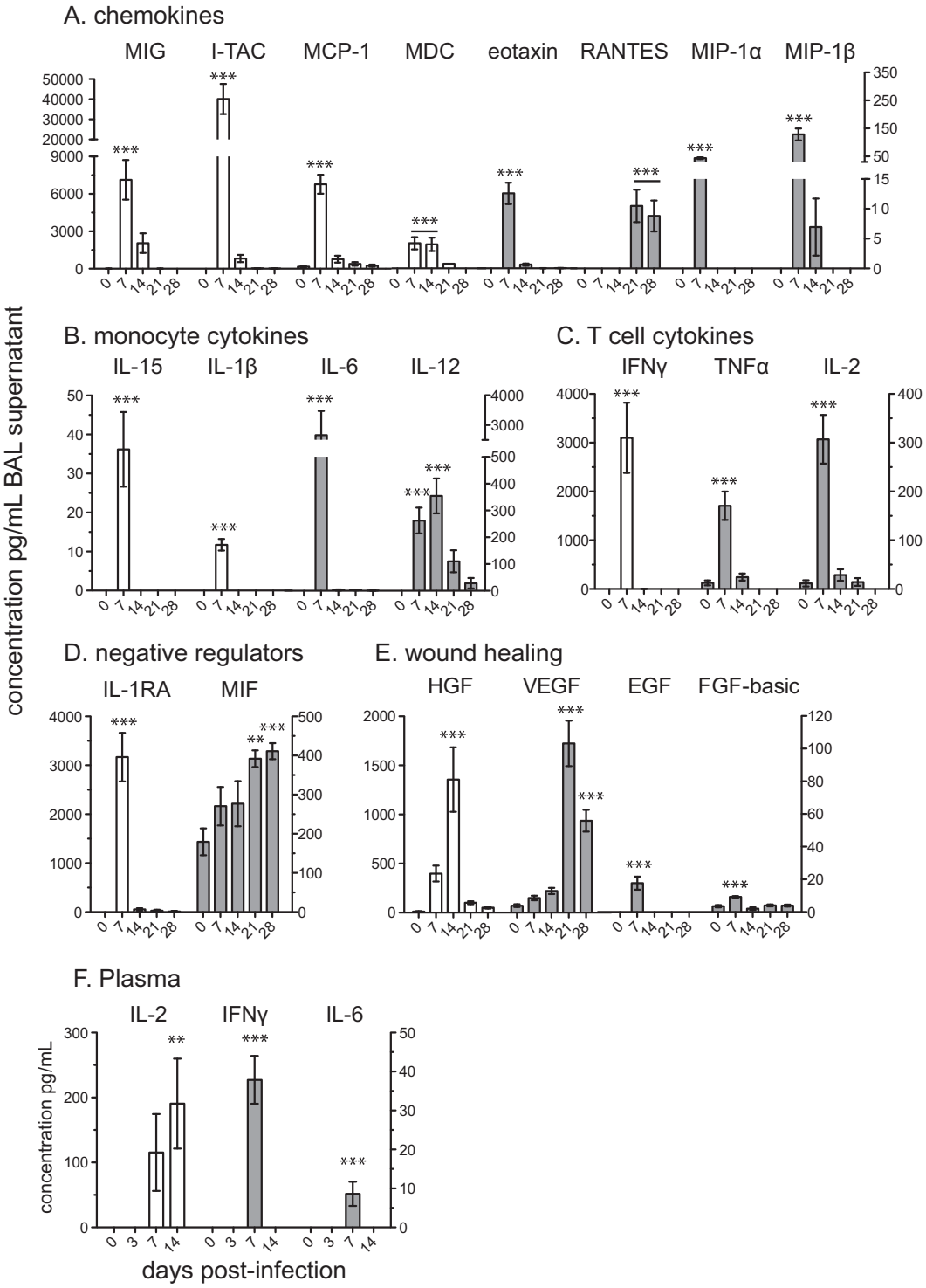

FIG 2 Acute SVV infection results in increased chemokine, cytokine, and growth factor levels in the lungs. Chemokine, cytokine, and growth factor levels were determined using Luminex technology in BAL supernatant (A to E) and plasma (F). Left *y* axis (white bar) and right *y* axis (gray bar), mean pg/ml ± SEM (**, $P < 0.01$; ***, $P < 0.001$).

receptor agonist (IL-1RA), which prevents IL-1 from signaling through the IL-1 receptor (IL-1R) (46), increased significantly at 7 dpi ($P < 0.001$). On the other hand, the concentration of macrophage migration inhibitory factor (MIF), which suppresses anti-inflammatory effects of glucocorticoids, steadily increased from 7 dpi and peaked at 28 dpi ($P < 0.001$) (47).

SVV acute infection also led to the upregulation of wound healing and growth factors in the lungs (Fig. 2E). Epidermal

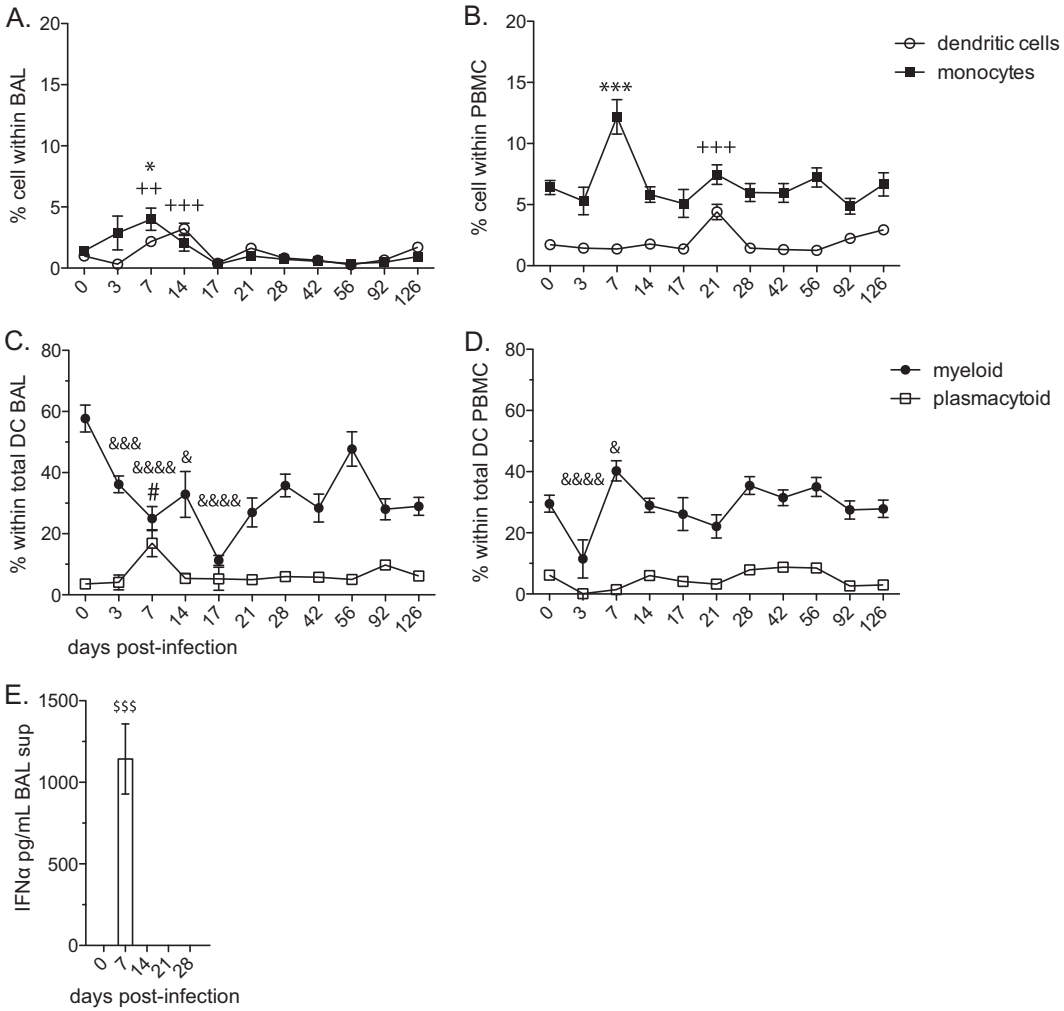

FIG 3 The frequency of plasmacytoid DCs increases early during acute SVV infection in the lungs. The frequencies (means ± SEM) of dendritic cells (DCs; lin$^-$ CD14$^-$ HLA-DR$^+$) and monocytes (lin$^-$ CD14$^+$ HLA-DR$^-$) in BAL cells (A) and PBMC (B) were measured by flow cytometry (++, $P < 0.01$; +++, $P < 0.001$ for DCs) (*, $P < 0.05$; ***, $P < 0.001$ for monocytes). The frequencies (means ± SEM) of myeloid DCs (mDCs; CD123$^-$ CD11c$^+$) and plasmacytoid DCs (pDCs; CD123$^+$ CD11c$^-$) in BAL cells (C) and PBMC (D) were measured by flow cytometry (&, $P < 0.05$; &&&, $P < 0.001$; &&&&, $P < 0.0001$ for mDC) (#, $P < 0.05$ for pDC). (E) The concentration of IFN-α was determined by IFN-α ELISA in BAL supernatant, mean pg/ml ± SEM ($$$, $P < 0.001$).

growth factor (EGF), which stimulates cell growth, proliferation, and differentiation (48), and FGF-b, a multifunctional protein involved in angiogenesis and wound healing (49), were significantly expressed at 7 dpi ($P < 0.001$) in BAL supernatant. Peak levels of hepatocyte growth factor (HGF), which regulates cell growth, cell motility, and morphogenesis and acts primarily upon epithelial and endothelial cells (50), were detected at 14 dpi ($P < 0.001$). Finally, an increased level of vascular endothelial growth factor (VEGF), which stimulates angiogenesis (51), was detected at 21 dpi ($P < 0.001$) and 28 dpi ($P < 0.001$).

In contrast to BAL supernatant, we were able to detect significant changes only in the levels of IL-2, IL-6, and IFN-γ in plasma following SVV infection (Fig. 2F). IL-6 and IFN-γ both significantly increased 7 dpi ($P < 0.001$), while IL-2 plasma levels peaked at 14 dpi ($P < 0.01$).

The frequency of plasmacytoid DCs increases early during acute SVV infection and correlates with IFN-α levels in the lungs. Given the increased levels of chemokines involved in monocyte/macrophage and DC recruitment as well as cytokines produced by these subsets, we characterized changes in their frequency in BAL cells (Fig. 3A) and PBMC (Fig. 3B). The frequency of DCs in BAL samples significantly increased at 7 ($P < 0.01$) and 14 ($P < 0.001$) dpi compared to baseline, and the frequency returned to the preinfection level by 17 dpi. Similarly, the frequency of DCs in PBMC were low but significantly increased at 21 dpi ($P < 0.001$) compared to that at day 0. The frequency of monocytes in BAL samples increased at 3 and 7 ($P < 0.05$) dpi, followed by a decrease in frequency to preinfection levels between 14 and 17 dpi. The frequency of monocytes in PBMC increased significantly at 7 dpi ($P < 0.001$) and returned to baseline levels by 14 dpi. We also examined changes in the two major DC subpopulations, myeloid DCs (mDC) and plasmacytoid DCs (pDCs) (Fig. 3C and D). In BAL cells, we detected a significant increase in the frequency of pDCs at 7 dpi ($P < 0.05$). The increase in pDC frequency was accompanied by a concomitant decrease in mDC frequency at 7 dpi in BAL cells. In PBMC, we did not detect any significant

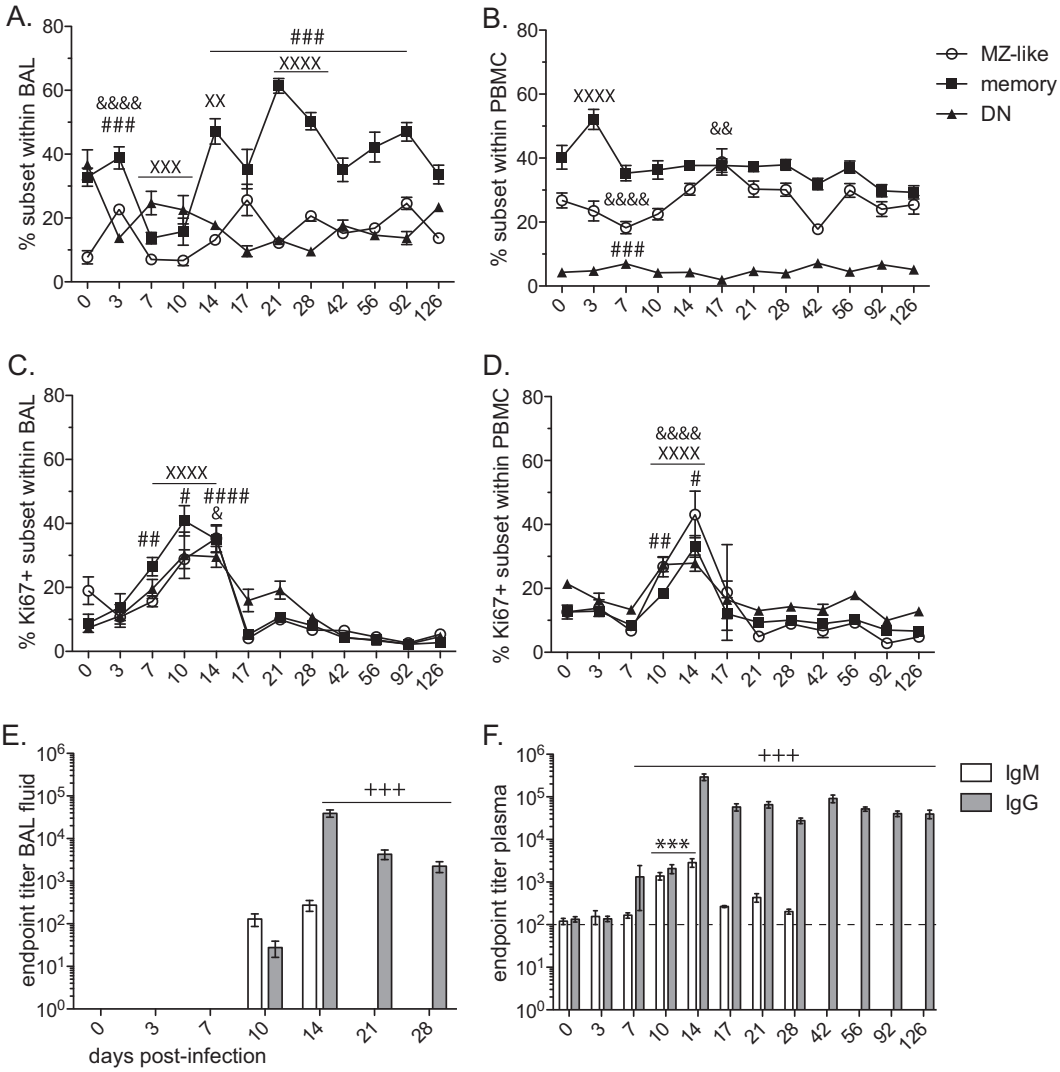

FIG 4 Acute SVV infection elicits B cell proliferation and antibody production in the lungs. The frequency (mean ± SEM) of marginal zone (MZ)-like (IgD^+ $CD27^+$), class-switched memory (IgD^- $CD27^+$), and double-negative (DN; IgD^- $CD27^-$) B cells was measured in BAL (A) and PBMC (B) samples by flow cytometry. Proliferation (means ± SEM) of B cell subsets was measured by detection of Ki67 in BAL (C) and PBMC (D) by flow cytometry (&, $P < 0.05$; &&, $P < 0.01$; &&&&, $P < 0.0001$ for MZ-like) (XX, $P < 0.01$; XXX, $P < 0.001$; XXXX, $P < 0.0001$ for memory) (#, $P < 0.05$; ##, $P < 0.01$; ###, $P < 0.001$; ####, $P < 0.0001$ for DN). SVV-specific IgM and IgG antibody endpoint titers (means ± SEM) were measured by standard ELISA in BAL supernatant (E) and plasma (F) (***, $P < 0.001$ for IgM) (+++, $P < 0.001$ for IgG).

changes in pDC frequency; however, we detected a significant decrease in mDC frequency at 3 dpi ($P < 0.0001$), followed by a significant increase at 7 dpi ($P < 0.05$), and the frequency returned to baseline by 10 dpi.

Given that activated pDCs play an important role in antiviral immunity through the production of type I interferon (52) and that we detected an increase in pDC frequency after SVV infection in the lungs, we investigated the levels of IFN-α by ELISA. Consistent with the observed increase in pDCs, our analysis showed a significant increase in the concentration of IFN-α at 7 dpi ($P < 0.001$) in BAL supernatant (Fig. 3E).

Acute SVV infection elicits B cell proliferation and antibody production in the lungs. To characterize the humoral immune response, we examined changes in the frequency and proliferative capacity of B cell subsets, as well as the production of SVV-specific IgM and IgG antibodies following SVV infection (Fig. 4). Following antigen encounter, naive B cells differentiate, undergo a proliferative burst, and acquire memory phenotype. Memory B cell subsets can be delineated into the following groups based on the expression of IgD and CD27: (i) marginal zone (MZ)-like (IgD^+ $CD27^+$), (ii) class-switched memory (IgD^- $CD27^+$), and (iii) double-negative (DN; IgD^- $CD27^-$) (53, 54). In BAL samples, the frequency of MZ-like B cells increased at 3 dpi ($P < 0.0001$), followed by a return to baseline levels at 7 dpi (Fig. 4A). The frequency of the class-switched memory B cell population initially decreased at 7 to 10 dpi ($P < 0.001$) and then increased to the peak level at 21 dpi ($P < 0.0001$) before returning to the baseline level at day 42 postinfection (Fig. 4A). The relative frequency of the DN B cell population decreased at 3 dpi ($P < 0.001$) and remained significantly below preinfection levels until 126 dpi (Fig. 4A). In PBMC (Fig. 4B), the frequency of MZ-like B cells initially decreased at 7 dpi ($P < 0.0001$), followed by an increase in fre-

quency, peaking at 17 dpi ($P < 0.01$). A marked increase in the frequency of memory B cells was observed at 3 dpi ($P < 0.0001$), while the frequency of DN B cells, albeit low, significantly increased at 7 dpi ($P < 0.001$).

Proliferation and clonal expansion of antigen-specific lymphocytes are critical for mediating protective immunity and the development of immunological memory. To monitor B cell proliferation following SVV infection, we measured changes in the expression of Ki67, a nuclear protein expressed during all active phases of cell division but absent in quiescent cells and during DNA repair (55). Although some $Ki67^+$ cells might not be antigen specific and are induced to undergo bystander activation/proliferation, determining changes in the kinetics and magnitude of Ki67 expression provides insight into the quality and quantity of the immune response to infection (56), vaccination (57), and cancer (58). Therefore, we determined the kinetics and magnitude of lymphocyte proliferation following SVV infection by measuring changes in the frequency of $Ki67^+$ cells within MZ-like, memory, and DN B cells (Fig. 4C and D). In BAL cells, B cell proliferation began at 7 dpi, peaked between 10 and 14 dpi, and returned to baseline levels by 17 dpi within all memory subsets (Fig. 4C). B cell proliferation was delayed in PBMC compared to that in BAL cells, beginning at 10 dpi, peaking at 14 dpi, and returning to baseline levels by approximately 17 dpi for all three subsets (Fig. 4D).

In accordance with the kinetics of the B cell proliferative burst, we were able to detect SVV-specific IgM and IgG antibodies in BAL fluid (Fig. 4E). IgM antibodies were detected only at 10 and 14 (average titer, 240 ± 71; $P < 0.05$) dpi, while IgG titers were detected at 10 dpi, peaked at 14 dpi (average titer, 1:39,300 ± 7,470; $P < 0.001$), and decreased at 21 and 28 dpi. Unfortunately, no further samples of BAL fluid were available past 28 dpi. In plasma (Fig. 4F), SVV-specific IgM titers were detected at 10 dpi and peaked at 14 dpi (average titer, 1:2,878 ± 657; $P < 0.001$) before declining to background levels at 17 dpi (Fig. 4F). SVV-specific IgG titers in plasma were first detected at 7 dpi, peaked at 14 dpi (average titer, 1:292,345 ± 50,575; $P < 0.001$), decreased slightly, and remained stable for the duration of the study.

Acute SVV infection induces robust proliferation of CD4 and CD8 T cells in the lungs. We next investigated the cellular immune response to SVV infection. Following antigen encounter, naive T cells become activated and differentiate into central memory (CM; $CD95^+$ $CD28^+$ $CCR7^+$), transitional effector memory (TEM; $CD95^+$ $CD28^+$ $CCR7^-$), and effector memory (EM; $CD95^+$ $CD28^-$ $CCR7^-$) T cells. To better define the T cell immune response to SVV infection, we monitored the frequency of these T cell subsets within the CD4 and CD8 T cell populations in BAL cells and PBMC (Fig. 5A to D).

In BAL samples, a significant increase in the frequency of CD4 CM T cells was observed between 3 and 17 dpi (Fig. 5A). Conversely, the frequency of TEM decreased at 7 dpi ($P < 0.0001$) and remained statistically lower than baseline until after 42 dpi (Fig. 5A). No significant changes in the frequency of CD4 EM T cells were detected post-SVV infection in the lungs (Fig. 5A). In PBMC, a decrease in CD4 CM T cells was accompanied by an increase in TEM cells at 3 and 21 dpi, while similar to BAL cells, no significant changes were observed in the frequency of CD4 EM T cells (Fig. 5B). Within the CD8 T cell subset in BAL samples, the relative percentage of CD8 EM cells increased significantly at 14 dpi ($P < 0.0001$), which was accompanied by a significant decrease in the frequency of CD8 TEM cells ($P < 0.0001$) (Fig. 5C). This redistribution of cells remained stable for the remainder of the study. CD8 CM T cells in BAL samples showed an increase at 7 dpi ($P < 0.001$) and thereafter remained stable throughout SVV infection (Fig. 5C). In PBMC, we detected an increase in the CD8 EM T cell subset frequency ($P < 0.01$), which was accompanied by a reciprocal decrease in the frequency of CD8 CM T cells at 3 dpi ($P < 0.0001$), while the TEM subset remained stable (Fig. 5D).

As described above for B cells, we assessed the kinetics and magnitude of T cell proliferation in BAL and PBMC by measuring the frequency of Ki67-positive cells within the CD4 and CD8 T cell subsets (Fig. 5E to H). In BAL cells, a significant proliferative burst in all CD4 T cell subsets was detected at 7, 10, and14 dpi ($P < 0.0001$) (Fig. 5E). In PBMC, we observed similar proliferative kinetics in all three CD4 subsets; however, the magnitude of the CD4 T cell proliferative burst was larger in BAL cells than in PBMC (AUC $P < 0.01$ for all subsets) (Fig. 5F). Similar to CD4 T cell subsets in BAL, significant CD8 T cell proliferation was observed between 7 and 14 dpi for all three subsets ($P < 0.0001$) (Fig. 5G). CD8 T cell proliferation in PBMC also occurred between 7 and 14 dpi, with a markedly reduced magnitude compared to that observed in BAL cells (AUC $P < 0.05$ for all subsets) (Fig. 5H).

The frequency of SVV-specific CD4 T is greater than CD8 T cells following acute infection in the lungs. We determined the frequency of SVV-specific CD4 and CD8 T cells by measuring the frequency of IFN-γ-, TNF-α-, MIP-1β-, and IL-2-producing cells in BAL (Fig. 6) and PBMC (Fig. 7) samples following stimulation with SVV lysate or an overlapping peptide pool covering SVV ORFs 4, 11, 16, 31, and 37 using intracellular cytokine staining (ICS).

Following stimulation with viral lysate, SVV-specific CD4 T cells producing IFN-γ (Fig. 6A), TNF-α (Fig. 6C), MIP-1β (Fig. 6E), and IL-2 (Fig. 6G) were first detected at 7 dpi in BAL samples, and their frequency peaked at 21 dpi. Although the kinetics of CD4 T cell responses to SVV peptides were similar to those detected following stimulation with lysate, the frequency of responding CD4 T cells was significantly lower (AUC $P < 0.01$) (Fig. 6B, D, F, H). In contrast to CD4 T cells, the frequency of SVV-specific CD8 T cells following stimulation with viral lysate compared to peptides was considerably lower in BAL samples than in PBMC samples (AUC $P < 0.05$ for IFN-γ, MIP-1β, and IL-2) (Fig. 6A, C, E, G). This difference might be due to the fact that SVV lysate is preferentially processed and presented via the major histocompatibility complex (MHC) class II pathway to CD4 T cells. Following stimulation with SVV peptide pools, SVV-specific CD8 T cells producing IFN-γ (Fig. 6B), TNF-α (Fig. 6D), and MIP-1β (Fig. 6F) were detected starting at 7 dpi, and their frequency peaked at 21 dpi ($P < 0.0001$) in BAL samples.

Overall, SVV-specific CD4 and CD8 T cell responses in PBMC were markedly reduced compared to those observed in BAL samples. In contrast to our observation in BAL, SVV-specific CD4 T cell responses following stimulation with lysate were noticeably reduced compared to CD8 T cell responses in PBMC (AUC $P < 0.01$ for TNF-α and MIP-1β) (Fig. 7). The peak response of SVV-specific CD8 T cells following stimulation with viral lysate was at 7 dpi for all four cytokines. The T cell response following stimulation with viral peptides in PBMC was significantly reduced compared to that measured with lysate.

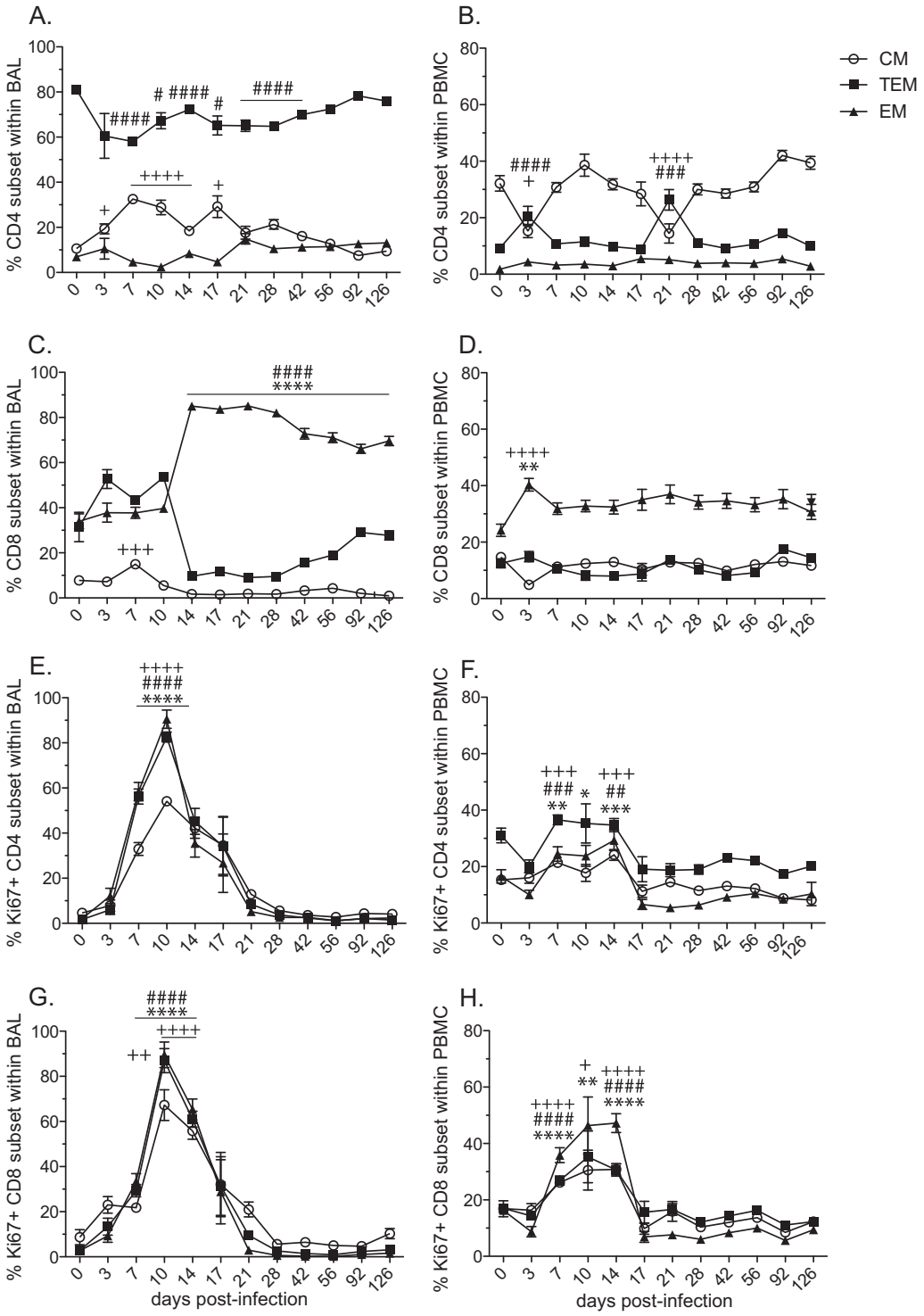

FIG 5 Acute SVV infection induces robust proliferation of CD4 and CD8 T cells in the lungs. The frequencies (means ± SEM) of central memory (CM; $CD95^+$ $CD28^+$ $CCR7^+$), transitional effector memory (TEM; $CD95^+$ $CD28^+$ $CCR7^-$), and effector memory (EM; $CD95^+$ $CD28^-$ $CCR7^-$) subsets in CD4 (A, B) and CD8 (C, D) T cells in BAL cells (A, C) and PBMC (B, D) were measured by flow cytometry. Proliferation (mean ± SEM) of T cell subsets was measured by the expression of Ki67 in CD4 (E, F) and CD8 (G, H) T cells in BAL cells (E, G) and PBMC (F, H) (+, $P < 0.05$; ++, $P < 0.01$; +++, $P < 0.001$; ++++, $P < 0.0001$ for CM) (#, $P < 0.05$; ##, $P < 0.01$; ###, $P < 0.001$; ####, $P < 0.0001$ for TEM) (*, $P < 0.05$; **, $P < 0.01$; ***, $P < 0.001$; ****, $P < 0.0001$ for EM).

Acute SVV infection results in upregulation of granzyme B in CD4 and CD8 T cell subsets in the lungs. We next determined the frequency of T cells with cytolytic potential by measuring the expression of granzyme B in CD4 and CD8 T cell subsets in lung and peripheral blood (Fig. 8). In BAL cells, we detected a significant increase in granzyme B expression at 7 dpi in CD4 CM ($P < 0.01$), TEM ($P < 0.0001$), and EM ($P < 0.0001$) T cell subsets, returning to baseline levels at 10 dpi (Fig. 8A). In PBMC, the frequency of

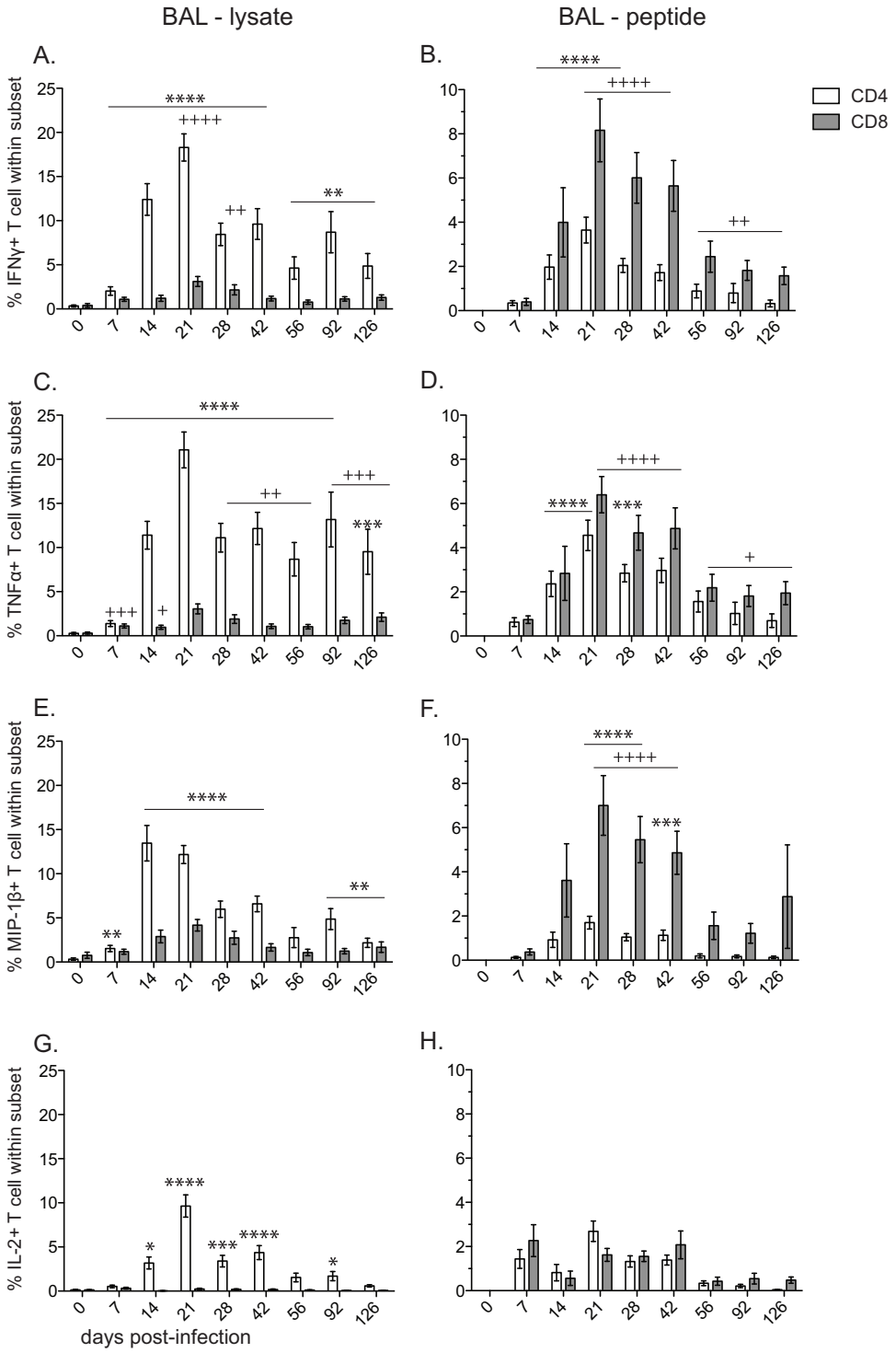

FIG 6 Frequency of SVV-specific CD4 T and CD8 T cells following acute infection in the lungs. The frequencies (means ± SEM) of SVV-specific CD4 (white bar) and CD8 (gray bar) T cells in BAL samples producing IFN-γ (A and B), TNF-α (C and D), MIP-β (E and F), and IL-2 (G and H) were measured by intracellular cytokine staining following stimulation with SVV lysate (A, C, E, G) or SVV overlapping peptide pool (B, D, F, H) (ORFs 4, 9, 11, 16, and 31) (*, $P < 0.05$; **, $P < 0.01$; ***, $P < 0.001$; ****, $P < 0.0001$ for CD4) (+, $P < 0.05$; ++, $P < 0.01$; +++, $P < 0.001$; ++++, $P < 0.0001$ for CD8).

granzyme B-positive CD4 EM T cells peaked at 3 dpi ($P < 0.001$) and decreased steadily, returning to baseline frequency at the end of the study (Fig. 8B). No changes were detected in granzyme B expression in CD4 TEM or EM T cells in PBMC. The expression of granzyme B differed considerably between CD4 and CD8 T cell subsets in BAL samples. While the frequency of granzyme B-positive CD8 CM T cells did not change throughout the study, the frequency of granzyme B-positive CD8 TEM T cells significantly

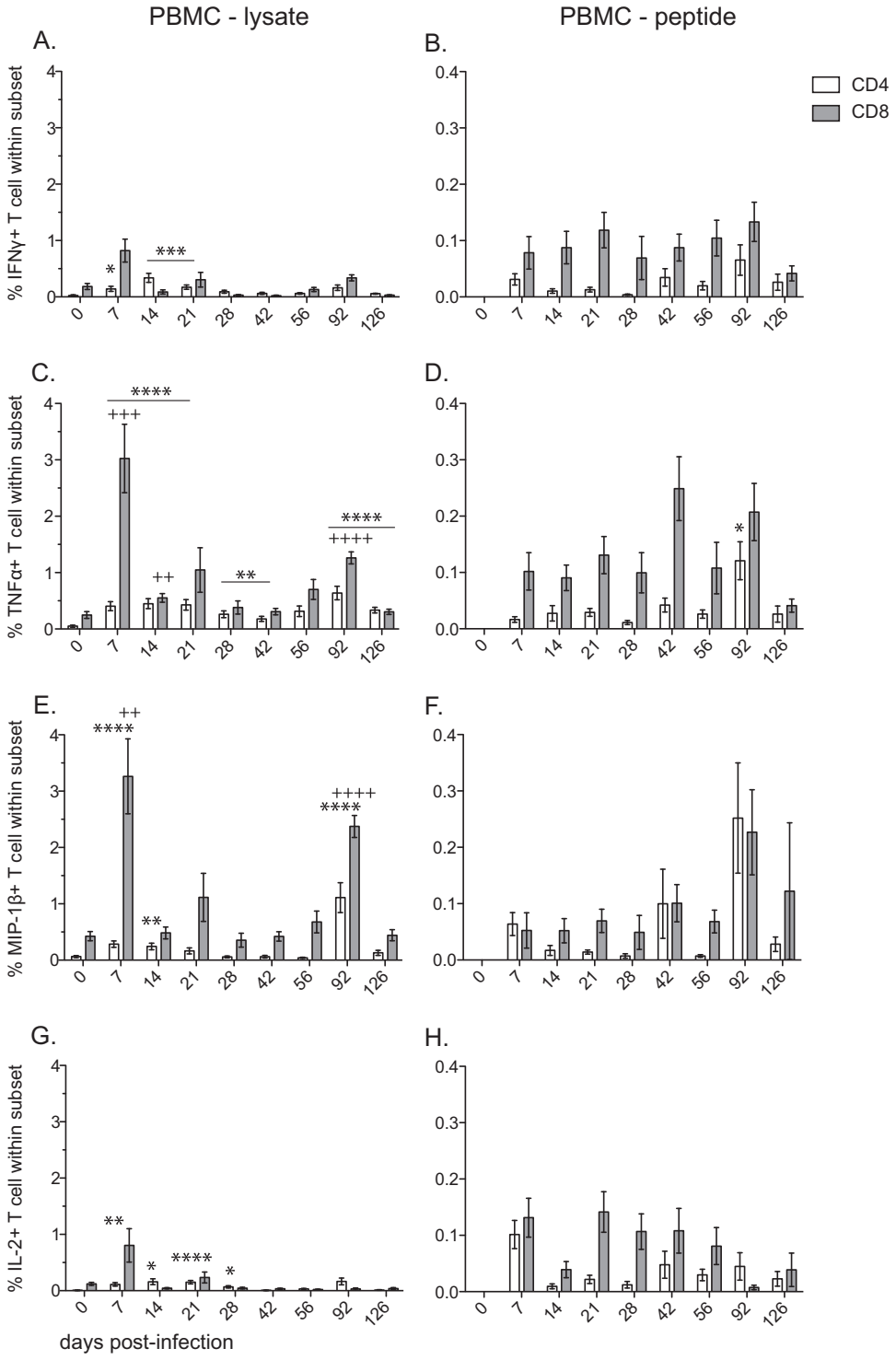

FIG 7 Frequency of SVV-specific CD4 T and CD8 T cells following acute infection in PBMC. The frequencies (means ± SEM) of SVV-specific CD4 (white bar) and CD8 (gray bar) T cells in PBMC samples producing IFN-γ (A and B), TNF-α (C and D), MIP-β (E and F), and IL-2 (G and H) were measured by intracellular cytokine staining following stimulation with SVV lysate (A, C, E, G) or an SVV overlapping peptide pool (B, D, F, H) (ORFs 4, 9, 11, 16, and 31) (*, $P < 0.05$; **, $P < 0.01$; ***, $P < 0.001$; ****, $P < 0.0001$ for CD4) (++, $P < 0.01$; +++, $P < 0.001$; ++++, $P < 0.0001$ for CD8).

increased at 7 ($P < 0.01$) and 10 ($P < 0.0001$) dpi before returning to baseline levels at 14 dpi. The frequency of granzyme B-positive CD8 EM T cells increased by 3 dpi, peaked at 14 dpi ($P < 0.0001$), and remained significantly higher than baseline for the rest of the study (Fig. 8C). Similar to CD4 EM T cells in PBMC, granzyme B expression in CD8 EM T cells peaked between 3 and 14 dpi and returned to baseline levels by 21 dpi (Fig. 8D). Expression of granzyme B in CD8 TEM and EM T cells peaked

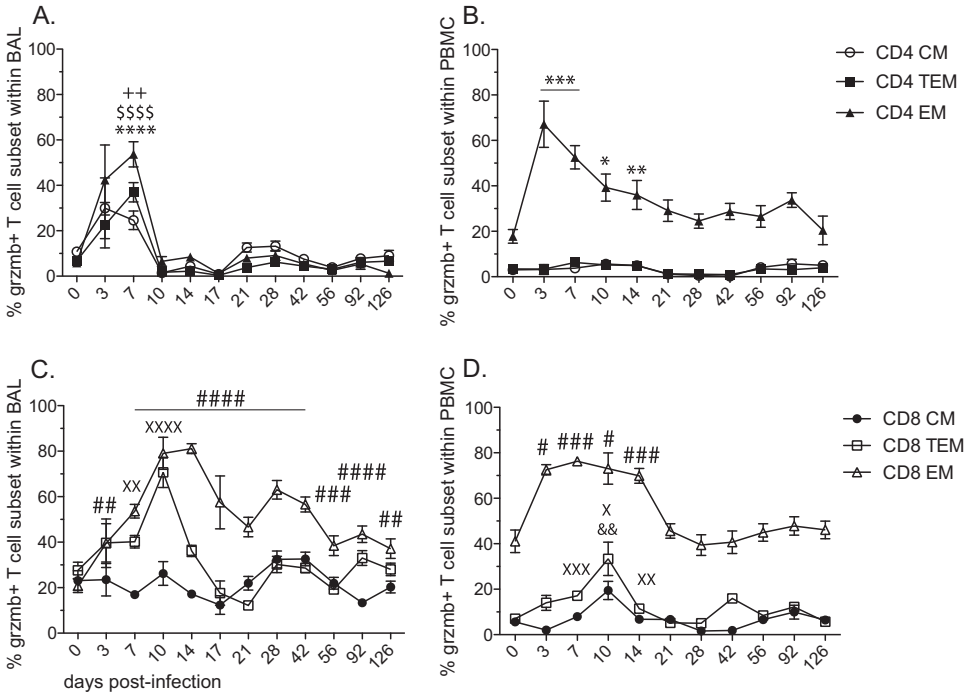

FIG 8 Acute SVV infection results in upregulation of granzyme B in CD4 and CD8 T cell subsets in the lungs. The frequencies (means ± SEM) of granzyme B-positive T cells within CM, TEM, and EM subsets of CD4 (A and B) and CD8 (C and D) T cells were assessed by flow cytometry in BAL cells (A and C) and PBMC (B and D) (++, $P < 0.01$for CD4 CM) ($$$$, $P < 0.0001$ for CD4 TEM) (*, $P < 0.05$; **, $P < 0.01$; ***, $P < 0.001$; ****, $P < 0.0001$ for CD4 EM) (&&, $P < 0.01$ for CD8 CM) (X, $P < 0.05$; XX, $P < 0.01$; XXX, $P < 0.001$; XXXX, $P < 0.0001$ for CD8 TEM) (#, $P < 0.05$; ##, $P < 0.01$; ###, $P < 0.001$; ####, $P < 0.0001$ for CD8 EM).

at 10 dpi ($P < 0.05$ and $P < 0.01$, respectively), returning to baseline levels by 21 dpi.

DISCUSSION

Primary infection with varicella-zoster virus (VZV) occurs mainly at the respiratory epithelium (1–3). Although numerous case studies have documented varicella pneumonia in adults during primary infection as well as the presence of VZV DNA in BAL fluid during reactivation (6, 59–61), the difficulty associated with obtaining human respiratory mucosal samples has resulted in an incomplete understanding of the immune response to VZV infection in the lung. Previous studies from our laboratory have demonstrated that intrabronchial infection of rhesus macaques with the closely related simian varicella virus (SVV) recapitulates the hallmarks of VZV infection in humans (25). Therefore, in this study, we utilized the rhesus macaque animal model to address the gap in knowledge.

Following SVV infection, and as described previously for pathogenic influenza infection (62, 63), neutrophils and lymphocytes rapidly infiltrate into the bronchoalveolar space. This is accompanied by a robust induction of several key T cell chemokines, notably MIG, I-TAC, MCP-1, MIP-1α, and MIP-1β. Interestingly, the number of circulating lymphocytes and neutrophils in the blood was significantly but transiently reduced, which suggests potential recruitment of T cells and neutrophils from peripheral blood to the lungs. These observations are in line with data from early clinical studies in children with varicella that documented an initial decrease in lymphocyte numbers shortly before varicella, followed by an increase after the appearance of rash (64, 65). Similarly, lymphopenia was reported in rhesus macaques infected with H5N1 influenza virus and coincided with the increased expression of T cell markers in the lungs, which also suggests T cell recruitment to the lungs during virus-induced respiratory disease (63). We also observed increased frequencies of monocytes and DCs in BAL samples on days 7 and 14 postinfection, correlating with an increase in chemokines that recruit these cell types, MCP-1 and MDC. The increase in monocytes may account for the observed increased levels at 7 dpi of IL-6 and IL-1β, cytokines involved in inflammation and infection responses. Similarly, we detected a significant increase in the concentration of IL-6 in plasma coinciding with a peak frequency of monocytes in PBMC at 7 dpi.

We also detected increased concentrations of Th1 cytokines IFN-γ, IL-12, and TNF-α but not Th2 cytokines (IL-4, IL-5, or IL-10) or the Th17 cytokine IL-17 in BAL supernatant after SVV infection, suggesting that the response to SVV in the lungs is mediated primarily by a CD4 Th1 response. Peak concentration of IL-2, necessary for proliferation and differentiation of T cells, was detected 3 days prior to peak proliferation of CD4 and CD8 T cells in the lung. IL-15, which is important for CD8 EM differentiation, reached peak levels shortly before a significant increase in frequency of CD8 EM T cells in the lungs. The increase in the T cell chemokine RANTES also correlates with the increased frequency of CD8 EM T cells in BAL samples. Increased BAL levels of IL-12, which plays a role in enhancing T cell cytotoxic function, coincided with increased expression of the cytolytic molecule granzyme B in CD8 and CD4 T cells.

Lastly, we detected increased levels of many growth factors that can play an important role in repairing tissue damage caused by

viral replication, notably FGF-basic and VEGF, which are involved in angiogenesis and wound healing, as well as EGF and HGF, which can stimulate cell growth, proliferation, and differentiation (48–51). These factors may have been produced by white blood cells that are either recruited to or activated at a site of injury and inflammation and/or by the organ in response to cell damage. The concentrations of the negative regulators IL-1RA and MIF were also significantly increased in BAL supernatant, most likely to facilitate the conclusion of the acute inflammatory phase.

SVV infection induces an upregulation of plasmacytoid DCs (pDCs) and a corresponding increase in IFN-α production. While IFN-α is produced by many cell types and in response to VZV infection (66, 67), pDCs selectively express Toll-like receptors (TLR) 7 and 9, which respond to viral nucleic acid through the MyD88-dependent pathway (68–70), eventually culminating in the production of copious amounts of the antiviral cytokine IFN-α (52, 71, 72). Indeed, pDCs may provide the first line of innate defense at mucosal sites of herpes simplex virus 2 (HSV-2) infection in a mouse model (72). Production of IFN-α was also shown to be critical in the control of VZV replication in the skin using the humanized SCID mouse model (16). Moreover, there is evidence that pDCs can activate both naive and memory T cells (73, 74), as well as present both endogenous antigens derived from viruses and exogenous antigen to promote the T cell response (75–79). Finally, pDCs may be important in the expansion and differentiation of Th1 responses (80), including following HSV-1 infection of mice (81). Our observations support these proposed roles for pDCs during viral infection with herpesviruses in nonhuman primates. The increased levels of IFN-α peaked just before a significant drop in SVV viral loads and likely contribute to the cessation of SVV replication. The increased frequency of pDCs also corresponds with the initiation of the T cell proliferative burst, suggesting that pDCs in the lung may initiate the cellular immune response. Elevated IFN-α levels also correlated with increased Th1 cytokines (IFN-γ, TNF-α, and IL-12) in BAL samples, supporting a role for pDCs in the initiation of Th1 CD4 responses.

We also report that SVV infection results in a 2-fold increase in the frequency of CD8 T cells in the BAL, which persisted for 4 months. We also detected a significant increase of CD8 EM T cells and a decrease in CD8 TEM, indicative of CD8 T cell differentiation. However, since the number of total lymphocytes collected in the BAL returned to baseline by 21 dpi, these data indicate that SVV infection results in a selective recruitment and differentiation of CD8 T cells in the lung. These observations are similar to a previous report from our laboratory investigating the immune response to influenza virus in rhesus macaques, which also described a dominance of terminally differentiated CD8 T cells in the lungs of infected animals (82). These data suggest that viral infection in the lungs result in the preferential recruitment and differentiation of CD8 T cells regardless of their antigen specificity, resulting in high levels of bystander activation.

Although T cell proliferation peaks at 10 dpi, the frequency of SVV-specific T cells (as measured by ICS) does not peak until 21 dpi, suggesting that proliferation precedes and might be required for the acquisition of effector function by T cells. Examination of SVV-specific T cells by ICS revealed a higher frequency of antigen-specific CD4 T cells than CD8 T cells. This observation was unexpected given the comparable proliferative kinetics and magnitudes of CD4 and CD8 T cell subsets in BAL samples. This difference could be due to the nature of stimulation antigens. Use of SVV lysate not only favors antigen presentation to CD4 T cells, but it also allows for processing and presentation of a large portion of SVV antigens. On the other hand, while the use of peptides favors presentation to CD8 T cells, the 5 overlapping peptide pools (SVV ORFs 4, 11, 16, 31, and 37) that we used cover only 20% of the total T cell response to SVV during acute infection (29), likely limiting the analysis of the anti-SVV CD8 T cell response. However, previous studies from our laboratory have demonstrated that CD4 T cells are essential for the resolution of acute SVV infection (83). Therefore, the increased prevalence of SVV-specific T cells within the CD4 T cell subset is most likely a reflection of the critical role these cells perform in the anti-SVV response.

SVV infection also resulted in the acquisition of T cell cytolytic capacity, as indicated by the upregulation of granzyme B expression. Interestingly, we observed a transient increase in granzyme B expression in CD4 T cells, whereas granzyme B induction in CD8 TEM and EM T cells reached higher levels and was sustained much longer than in CD4 T cells. Together with the cytokine production, these data highlight fundamental differences in the differentiation programs of CD4 and CD8 EM T cells. These observations also indicate that T cells contribute to the primary antiviral immune response by producing essential cytokines (IFN-γ, TNF-α, MIP-1β, IL-2), as well as by killing infected cells.

We also report a robust production of SVV-specific IgG in BAL samples. Immunoglobulins in lung fluid can be derived from the blood by transudation or could be synthesized locally by cells within the lymphoid tissue in the respiratory tract. Furthermore, lung lining fluid antibodies are important in mucosal defense where the lungs are continually exposed to antigenic material, including during bacterial and viral infection (84–86). We detected both IgM and IgG SVV-specific antibodies in BAL fluid beginning at 10 dpi, which correlated with peak B cell proliferation and supports local secretion of antibodies. The presence of lung immunoglobulins could contribute to resolution of acute SVV infection through complement activation, opsonization, and antibody-dependent cell-mediated cytotoxicity by effector cells.

Taken together, the data presented here provide a comprehensive view of the kinetics of the immune response to SVV and its relationship to the resolution of acute infection in the lungs. Collectively, these data suggest that SVV infection is first controlled by innate immunity through production of antiviral cytokines, notably IFN-α. The significant production of chemokines and cytokines correlates with the recruitment of lymphocytes, neutrophils, and monocytes and an initial dramatic decline in viral load. The second and more gradual decline in viral load to undetectable levels is then mediated by adaptive immunity (granzyme B-mediated killing of infected cells, effector cytokine production by T cells and antibodies). Angiogenic (VEGF) and regulatory factors (MIF) are then produced to repair damage that occurred during infection and the ensuing immune response. Future studies will further define the role of CD4 and CD8 T cells during acute SVV infection, and these data will contribute to the development of more efficacious vaccines that can boost protective T cell responses against VZV.

ACKNOWLEDGMENTS

We thank the Division of Comparative Medicine at the Oregon National Primate Research Center for expert animal care, especially Alfred Legasse,

Miranda Fischer, and Shannon Planer for collection of blood and BAL samples.

This work was supported by NIH R01AG037042, 2T32AI007472-16, and NIH 8P51 OD011092-53.

REFERENCES

1. **Leclair JM, Zaia JA, Levin MJ, Congdon RG, Goldmann DA.** 1980. Airborne transmission of chickenpox in a hospital. N. Engl. J. Med. **302:**450–453.
2. **Sawyer MH, Chamberlin CJ, Wu YN, Aintablian N, Wallace MR.** 1994. Detection of varicella-zoster virus DNA in air samples from hospital rooms. J. Infect. Dis. **169:**91–94.
3. **Suzuki K, Yoshikawa T, Tomitaka A, Matsunaga K, Asano Y.** 2004. Detection of aerosolized varicella-zoster virus DNA in patients with localized herpes zoster. J. Infect. Dis. **189:**1009–1012. http://dx.doi.org/10.1086/382029.
4. **Grose C.** 1981. Variation on a theme by Fenner: the pathogenesis of chickenpox. Pediatrics **68:**735–737.
5. **Heininger U, Seward JF.** 2006. Varicella. Lancet **368:**1365–1376. http://dx.doi.org/10.1016/S0140-6736(06)69561-5.
6. **Mohsen AH, McKendrick M.** 2003. Varicella pneumonia in adults. Eur. Respir. J. **21:**886–891. http://dx.doi.org/10.1183/09031936.03.00103202.
7. **Chiner E, Ballester I, Betlloch I, Blanquer J, Aguar MC, Blanquer R, Fernandez-Fabrellas E, Andreu AL, Briones M, Sanz F.** 2010. Varicella-zoster virus pneumonia in an adult population: has mortality decreased?. Scand. J. Infect. Dis. **42:**215–221. http://dx.doi.org/10.3109/00365540903428166.
8. **Cohen JI, Straus SE, Arvin AM.** 2007. Varicella-zoster virus replication, pathogenesis, and management, p 2773–2818. *In* Knipe DM, Howley PM, Griffin DE, Lamb RA, Martin MA, Roizman B, Straus SE (ed), Fields virology, 5th ed, vol 2. Lippincott Williams & Wilkins, Philadelphia, PA.
9. **Saulsbury FT.** 1991. Varicella pneumonia as the presenting manifestation of immunodeficiency. Clin. Pediatr. **30:**555–558. http://dx.doi.org/10.1177/000992289103000906.
10. **Deshmane SL, Kremlev S, Amini S, Sawaya BE.** 2009. Monocyte chemoattractant protein-1 (MCP-1): an overview. J. Interferon Cytokine Res. **29:**313–326. http://dx.doi.org/10.1089/jir.2008.0027.
11. **Morrow G, Slobedman B, Cunningham AL, Abendroth A.** 2003. Varicella-zoster virus productively infects mature dendritic cells and alters their immune function. J. Virol. **77:**4950–4959. http://dx.doi.org/10.1128/JVI.77.8.4950-4959.2003.
12. **Huch JH, Cunningham AL, Arvin AM, Nasr N, Santegoets SJ, Slobedman E, Slobedman B, Abendroth A.** 2010. Impact of varicella-zoster virus on dendritic cell subsets in human skin during natural infection. J. Virol. **84:**4060–4072. http://dx.doi.org/10.1128/JVI.01450-09.
13. **Moffat JF, Stein MD, Kaneshima H, Arvin AM.** 1995. Tropism of varicella-zoster virus for human CD4+ and CD8+ T lymphocytes and epidermal cells in SCID-hu mice. J. Virol. **69:**5236–5242.
14. **Ku C-C, Zerboni L, Ito H, Graham BS, Wallace M, Arvin AM.** 2004. Varicella-zoster virus transfer to skin by T cells and modulation of viral replication by epidermal cell interferon-{alpha}. J. Exp. Med. **200:**917–925. http://dx.doi.org/10.1084/jem.20040634.
15. **Ku CC, Padilla JA, Grose C, Butcher EC, Arvin AM.** 2002. Tropism of varicella-zoster virus for human tonsillar CD4(+) T lymphocytes that express activation, memory, and skin homing markers. J. Virol. **76:**11425–11433. http://dx.doi.org/10.1128/JVI.76.22.11425-11433.2002.
16. **Ku CC, Zerboni L, Ito H, Graham BS, Wallace M, Arvin AM.** 2004. Varicella-zoster virus transfer to skin by T cells and modulation of viral replication by epidermal cell interferon-alpha. J. Exp. Med. **200:**917–925. http://dx.doi.org/10.1084/jem.20040634.
17. **Parker DC.** 1993. The functions of antigen recognition in T cell-dependent B cell activation. Semin. Immunol. **5:**413–420.
18. **Arvin AM, Koropchak CM, Williams BR, Grumet FC, Foung SK.** 1986. Early immune response in healthy and immunocompromised subjects with primary varicella-zoster virus infection. J. Infect. Dis. **154:**422–429. http://dx.doi.org/10.1093/infdis/154.3.422.
19. **Jura E, Chadwick EG, Josephs SH, Steinberg SP, Yogev R, Gershon AA, Krasinski KM, Borkowsky W.** 1989. Varicella-zoster virus infections in children infected with human immunodeficiency virus. Pediatr. Infect. Dis. J. **8:**586–590. http://dx.doi.org/10.1097/00006454-198909000-00003.
20. **Zerboni L, Nader S, Aoki K, Arvin AM.** 1998. Analysis of the persistence of humoral and cellular immunity in children and adults immunized with varicella vaccine. J. Infect. Dis. **177:**1701–1704. http://dx.doi.org/10.1086/517426.
21. **Clarkson MJ, Thorpe E, McCarthy K.** 1967. A virus disease of captive vervet monkeys (*Cercopithecus aethiops*) caused by a new herpesvirus. Arch. Gesamte Virusforsch. **22:**219–234. http://dx.doi.org/10.1007/BF01240517.
22. **Fletcher TM, III, Gray WL.** 1993. DNA sequence and genetic organization of the unique short (US) region of the simian varicella virus genome. Virology **193:**762–773. http://dx.doi.org/10.1006/viro.1993.1185.
23. **Gray WL, Pumphrey CY, Ruyechan WT, Fletcher TM.** 1992. The simian varicella virus and varicella zoster virus genomes are similar in size and structure. Virology **186:**562–572. http://dx.doi.org/10.1016/0042-6822(92)90022-H.
24. **Gray WL, Starnes B, White MW, Mahalingam R.** 2001. The DNA sequence of the simian varicella virus genome. Virology **284:**123–130. http://dx.doi.org/10.1006/viro.2001.0912.
25. **Messaoudi I, Barron A, Wellish M, Engelmann F, Legasse A, Planer S, Gilden D, Nikolich-Zugich J, Mahalingam R.** 2009. Simian varicella virus infection of rhesus macaques recapitulates essential features of varicella zoster virus infection in humans. PLoS Pathog. **5:**e1000657. http://dx.doi.org/10.1371/journal.ppat.1000657.
26. **Meyer C, Kerns A, Barron A, Kreklywich C, Streblow DN, Messaoudi I.** 2011. Simian varicella virus gene expression during acute and latent infection of rhesus macaques. J. Neurovirol. **17:**600–612. http://dx.doi.org/10.1007/s13365-011-0057-y.
27. **National Research Council.** 2011. Guide for the care and use of laboratory animals, 8th ed. National Academies Press, Washington, DC.
28. **Gray WL, Zhou F, Noffke J, Tischer BK.** 2011. Cloning the simian varicella virus genome in *E. coli* as an infectious bacterial artificial chromosome. Arch. Virol. **156:**739–746. http://dx.doi.org/10.1007/s00705-010-0889-4.
29. **Haberthur K, Kraft A, Arnold N, Park B, Meyer C, Asquith M, Dewane J, Messaoudi I.** 2013. Genome-wide analysis of T cell responses during acute and latent simian varicella virus infections in rhesus macaques. J. Virol. **87:**11751–11761. http://dx.doi.org/10.1128/JVI.01809-13.
30. **Deshmane SL, Kremlev S, Amini S, Sawaya BE.** 2009. Monocyte chemoattractant protein-1 (MCP-1): an overview. J. Interferon Cytokine Res. **29:**313–326. http://dx.doi.org/10.1089/jir.2008.0027.
31. **Maurer M, von Stebut E.** 2004. Macrophage inflammatory protein-1. Int. J. Biochem. Cell Biol. **36:**1882–1886. http://dx.doi.org/10.1016/j.biocel.2003.10.019.
32. **Griffiths-Johnson DA, Collins PD, Rossi AG, Jose PJ, Williams TJ.** 1993. The chemokine, eotaxin, activates guinea-pig eosinophils *in vitro* and causes their accumulation into the lung *in vivo*. Biochem. Biophys. Res. Commun. **197:**1167–1172. http://dx.doi.org/10.1006/bbrc.1993.2599.
33. **Sallusto F, Palermo B, Hoy A, Lanzavecchia A.** 1999. The role of chemokine receptors in directing traffic of naive, type 1 and type 2 T cells. Curr. Top. Microbiol. Immunol. **246:**123–128.
34. **Forssmann U, Uguccioni M, Loetscher P, Dahinden CA, Langen H, Thelen M, Baggiolini M.** 1997. Eotaxin-2, a novel CC chemokine that is selective for the chemokine receptor CCR3, and acts like eotaxin on human eosinophil and basophil leukocytes. J. Exp. Med. **185:**2171–2176. http://dx.doi.org/10.1084/jem.185.12.2171.
35. **Yamashita U, Kuroda E.** 2002. Regulation of macrophage-derived chemokine (MDC, CCL22) production. Crit. Rev. Immunol. **22:**105–114.
36. **Liu MT, Armstrong D, Hamilton TA, Lane TE.** 2001. Expression of Mig (monokine induced by interferon-gamma) is important in T lymphocyte recruitment and host defense following viral infection of the central nervous system. J. Immunol. **166:**1790–1795. http://dx.doi.org/10.4049/jimmunol.166.3.1790.
37. **Liu MT, Chen BP, Oertel P, Buchmeier MJ, Armstrong D, Hamilton TA, Lane TE.** 2000. The T cell chemoattractant IFN-inducible protein 10 is essential in host defense against viral-induced neurologic disease. J. Immunol. **165:**2327–2330. http://dx.doi.org/10.4049/jimmunol.165.5.2327.
38. **Schall TJ, Bacon K, Toy KJ, Goeddel DV.** 1990. Selective attraction of monocytes and T lymphocytes of the memory phenotype by cytokine RANTES. Nature **347:**669–671. http://dx.doi.org/10.1038/347669a0.
39. **Dinarello CA.** 2005. Interleukin-1beta. Crit. Care Med. **33:**S460–462. http://dx.doi.org/10.1007/s10654-007-9169-3.
40. **Hirano T, Akira S, Taga T, Kishimoto T.** 1990. Biological and clinical aspects of interleukin 6. Immunol. Today **11:**443–449.
41. **Esposito E, Cuzzocrea S.** 2009. TNF-alpha as a therapeutic target in inflam-

matory diseases, ischemia-reperfusion injury and trauma. Curr. Med. Chem. **316:**3152–3167. http://dx.doi.org/10.2174/092986709788803024.
42. **Fehniger TA, Caligiuri MA.** 2001. Interleukin 15: biology and relevance to human disease. Blood. **97:**14–32. http://dx.doi.org/10.1182/blood.V97.1.14.
43. **Scott P.** 1993. IL-12: initiation cytokine for cell-mediated immunity. Science. **260:**496–497.
44. **Boehm U, Klamp T, Groot M, Howard JC.** 1997. Cellular responses to interferon-γ. Annu. Rev. Immunol. **15:**749–795.
45. **Liao W, Lin JX, Leonard WJ.** 2013. Interleukin-2 at the crossroads of effector responses, tolerance, and immunotherapy. Immunity **38:**13–25. http://dx.doi.org/10.1016/j.immuni.2013.01.004.
46. **Arend WP, Malyak M, Guthridge CJ, Gabay C.** 1998. Interleukin-1 receptor antagonist: role in biology. Annu. Rev. Immunol. **16:**27–55.
47. **Calandra T, Bucala R.** 1997. Macrophage migration inhibitory factor (MIF): a glucocorticoid counter-regulator within the immune system. Crit. Rev. Immunol. **117:**77–88.
48. **Carpenter G, Cohen S.** 1990. Epidermal growth factor. J. Biol. Chem. **265:**7709–7712.
49. **Yu PJ, Ferrari G, Galloway AC, Mignatti P, Pintucci G.** 2007. Basic fibroblast growth factor (FGF-2): the high molecular weight forms come of age. J. Cell. Biochem. **100:**1100–1108. http://dx.doi.org/10.1002/jcb.21116.
50. **Warn R.** 1994. Growth factors. A scattering of factors. Curr. Biol. **4:**1043–1045.
51. **Byrne AM, Bouchier-Hayes DJ, Harmey JH.** 2005. Angiogenic and cell survival functions of vascular endothelial growth factor (VEGF). J. Cell. Mol. Med. **9:**777–794. http://dx.doi.org/10.1111/j.1582-4934.2005.tb00379.x.
52. **Fitzgerald-Bocarsly P, Feldman M, Mendelsohn M, Curl S, Lopez C.** 1988. Human mononuclear cells which produce interferon-alpha during NK(HSV-FS) assays are HLA-DR positive cells distinct from cytolytic natural killer effectors. J. Leukoc. Biol. **43:**323–334.
53. **Kaminski DA, Wei C, Qian Y, Rosenberg AF, Sanz I.** 2012. Advances in human B cell phenotypic profiling. Front. Immunol. **3:**302. http://dx.doi.org/10.3389/fimmu.2012.00302.
54. **Tangye SG, Tarlinton DM.** 2009. Memory B cells: effectors of long-lived immune responses. Eur. J. Immunol. **39:**2065-2075. http://dx.doi.org/10.1002/eji.200939531.
55. **Gerdes J, Lemke H, Baisch H, Wacker HH, Schwab U, Stein H.** 1984. Cell cycle analysis of a cell proliferation-associated human nuclear antigen defined by the monoclonal antibody Ki-67. J. Immunol. **133:**1710–1715.
56. **Kaur A, Hale CL, Ramanujan S, Jain RK, Johnson RP.** 2000. Differential dynamics of CD4(+) and CD8(+) T-lymphocyte proliferation and activation in acute simian immunodeficiency virus infection. J. Virol. **74:**8413–8424. http://dx.doi.org/10.1128/JVI.74.18.8413-8424.2000.
57. **Li X, Miao H, Henn A, Topham DJ, Wu H, Zand MS, Mosmann TR.** 2012. Ki-67 expression reveals strong, transient influenza specific CD4 T cell responses after adult vaccination. Vaccine **30:**4581–4584. http://dx.doi.org/10.1016/j.vaccine.2012.04.059.
58. **Brown JR, DiGiovanna MP, Killelea B, Lannin DR, Rimm DL.** 2014. Quantitative assessment Ki-67 score for prediction of response to neoadjuvant chemotherapy in breast cancer. Lab. Invest. **94:**98–106. http://dx.doi.org/10.1038/labinvest.2013.128.
59. **Fraisse P, Faller M, Rey D, Labouret N, Partisani M, Stoll-Keller F, Lang JM, Weitzenblum E.** 1998. Recurrent varicella pneumonia complicating an endogenous reactivation of chickenpox in an HIV-infected adult patient. Eur. Respir. J. **11:**776–778.
60. **Saito S, Yano T, Koga H, Arikawa K, Koyanagi N, Oizumi K.** 1999. Case of varicella-zoster pneumonia with bronchioalveolar lavage confirmed by the detection of VZV DNA in the bronchial washing by the polymerase chain reaction. Kansenshogaku Zasshi **73:**346–350. (In Japanese.)
61. **Yasuo M, Yamamoto H, Maruyama Y.** 2002. An adult patient with varicella-zoster pneumonia while under inhaled steroid treatment. Nihon Kokyuki Gakkai Zasshi **40:**77–80. (In Japanese.)
62. **Zhang K, Xu W, Zhang Z, Wang T, Sang X, Cheng K, Yu Z, Zheng X, Wang H, Zhao Y, Huang G, Yang S, Qin C, Gao Y, Xia X.** 2013. Experimental infection of non-human primates with avian influenza virus (H9N2). Arch. Virol. **158:**2127–2134. http://dx.doi.org/10.1007/s00705-013-1721-8.
63. **Shinya K, Gao Y, Cilloniz C, Suzuki Y, Fujie M, Deng G, Zhu Q, Fan S, Makino A, Muramoto Y, Fukuyama S, Tamura D, Noda T, Eisfeld AJ, Katze MG, Chen H, Kawaoka Y.** 2012. Integrated clinical, pathologic, virologic, and transcriptomic analysis of H5N1 influenza virus-induced viral pneumonia in the rhesus macaque. J. Virol. **86:**6055–6066. http://dx.doi.org/10.1128/JVI.00365-12.
64. **Mitchell G, Fletcher G.** 1927. Studies on varicella. JAMA **89:**279–280.
65. **Holbrook A.** 1941. The blood picture in chickenpox. Arch. of Intern. Med. **68:**294–308.
66. **Yu HR, Huang HC, Kuo HC, Sheen JM, Ou CY, Hsu TY, Yang KD.** 2011. IFN-alpha production by human mononuclear cells infected with varicella-zoster virus through TLR9-dependent and -independent pathways. Cell. Mol. Immunol. **8:**181–188. http://dx.doi.org/10.1038/cmi.2010.84.
67. **Zerboni L, Sen N, Oliver SL, Arvin AM.** 2014. Molecular mechanisms of varicella zoster virus pathogenesis. Nat. Rev. Microbiol. **12:**197–210. http://dx.doi.org/10.1038/nrmicro3215.
68. **Hacker H, Vabulas RM, Takeuchi O, Hoshino K, Akira S, Wagner H.** 2000. Immune cell activation by bacterial CpG-DNA through myeloid differentiation marker 88 and tumor necrosis factor receptor-associated factor (TRAF)6. J. Exp. Med. **192:**595–600. http://dx.doi.org/10.1084/jem.192.4.595.
69. **Schnare M, Holt AC, Takeda K, Akira S, Medzhitov R.** 2000. Recognition of CpG DNA is mediated by signaling pathways dependent on the adaptor protein MyD88. Curr. Biol. **10:**1139–1142. http://dx.doi.org/10.1016/S0960-9822(00)00700-4.
70. **Hemmi H, Kaisho T, Takeuchi O, Sato S, Sanjo H, Hoshino K, Horiuchi T, Tomizawa H, Takeda K, Akira S.** 2002. Small anti-viral compounds activate immune cells via the TLR7 MyD88-dependent signaling pathway. Nat. Immunol. **3:**196–200. http://dx.doi.org/10.1038/ni758.
71. **Takagi H, Fukaya T, Eizumi K, Sato Y, Sato K, Shibazaki A, Otsuka H, Hijikata A, Watanabe T, Ohara O, Kaisho T, Malissen B, Sato K.** 2011. Plasmacytoid dendritic cells are crucial for the initiation of inflammation and T cell immunity in vivo. Immunity **35:**958–971. http://dx.doi.org/10.1016/j.immuni.2011.10.014.
72. **Lund JM, Linehan MM, Iijima N, Iwasaki A.** 2006. Cutting edge: plasmacytoid dendritic cells provide innate immune protection against mucosal viral infection in situ. J. Immunol. **177:**7510–7514. http://dx.doi.org/10.4049/jimmunol.177.11.7510.
73. **Colonna M, Trinchieri G, Liu YJ.** 2004. Plasmacytoid dendritic cells in immunity. Nat. Immunol. **5:**1219–1226. http://dx.doi.org/10.1038/ni1141.
74. **Liu YJ.** 2005. IPC: professional type 1 interferon-producing cells and plasmacytoid dendritic cell precursors. Annu. Rev. Immunol. **23:**275–306. http://dx.doi.org/10.1146/annurev.immunol.23.021704.115633.
75. **Di Pucchio T, Chatterjee B, Smed-Sorensen A, Clayton S, Palazzo A, Montes M, Xue Y, Mellman I, Banchereau J, Connolly JE.** 2008. Direct proteasome-independent cross-presentation of viral antigen by plasmacytoid dendritic cells on major histocompatibility complex class I. Nat. Immunol. **9:**551–557. http://dx.doi.org/10.1038/ni.1602.
76. **Fonteneau JF, Gilliet M, Larsson M, Dasilva I, Munz C, Liu YJ, Bhardwaj N.** 2003. Activation of influenza virus-specific CD4+ and CD8+ T cells: a new role for plasmacytoid dendritic cells in adaptive immunity. Blood **101:**3520–3526. http://dx.doi.org/10.1182/blood-2002-10-3063.
77. **Salio M, Palmowski MJ, Atzberger A, Hermans IF, Cerundolo V.** 2004. CpG-matured murine plasmacytoid dendritic cells are capable of *in vivo* priming of functional CD8 T cell responses to endogenous but not exogenous antigens. J. Exp. Med. **199:**567–579. http://dx.doi.org/10.1084/jem.20031059.
78. **Schlecht G, Garcia S, Escriou N, Freitas AA, Leclerc C, Dadaglio G.** 2004. Murine plasmacytoid dendritic cells induce effector/memory CD8+ T-cell responses *in vivo* after viral stimulation. Blood **104:**1808–1815. http://dx.doi.org/10.1182/blood-2004-02-0426.
79. **Young LJ, Wilson NS, Schnorrer P, Proietto A, ten Broeke T, Matsuki Y, Mount AM, Belz GT, O'Keeffe M, Ohmura-Hoshino M, Ishido S, Stoorvogel W, Heath WR, Shortman K, Villadangos JA.** 2008. Differential MHC class II synthesis and ubiquitination confers distinct antigen-presenting properties on conventional and plasmacytoid dendritic cells. Nat. Immunol. **9:**1244–1252. http://dx.doi.org/10.1038/ni.1665.
80. **Krug A, Veeraswamy R, Pekosz A, Kanagawa O, Unanue ER, Colonna M, Cella M.** 2003. Interferon-producing cells fail to induce proliferation of naive T cells but can promote expansion and T helper 1 differentiation of antigen-experienced unpolarized T cells. J. Exp. Med. **197:**899–906. http://dx.doi.org/10.1084/jem.20021091.
81. **Yoneyama H, Matsuno K, Toda E, Nishiwaki T, Matsuo N, Nakano A, Narumi S, Lu B, Gerard C, Ishikawa S, Matsushima K.** 2005. Plasmacytoid DCs help lymph node DCs to induce anti-HSV CTLs. J. Exp. Med. **202:**425–435. http://dx.doi.org/10.1084/jem.20041961.

82. **Sastre A, Katze MG, Messaoudi I.** 2012. Increased viral loads and exacerbated innate host responses in aged macaques infected with the 2009 pandemic H1N1 influenza A virus. J. Virol. **86:**11115–11127. http://dx.doi.org/10.1128/JVI.01571-12.
83. **Haberthur K, Engelmann F, Park B, Barron A, Legasse A, Dewane J, Fischer M, Kerns A, Brown M, Messaoudi I.** 2011. CD4 T cell immunity is critical for the control of simian varicella virus infection in a nonhuman primate model of VZV infection. PLoS Pathog. **7:**e1002367. http://dx.doi.org/10.1371/journal.ppat.1002367.
84. **Clay C, Donart N, Fomukong N, Knight JB, Lei W, Price L, Hahn F, Van Westrienen J, Harrod KS.** 2012. Primary severe acute respiratory syndrome coronavirus infection limits replication but not lung inflammation upon homologous rechallenge. J. Virol. **86:**4234–4244. http://dx.doi.org/10.1128/JVI.06791-11.
85. **Clarke LM, Sierra MF, Shahabbudin M, Cummings RV, Pellegrino MG, Steiner P, Volsky DJ, Nowakowski M.** 1992. Markers of human immunodeficiency virus infection in pediatric bronchoalveolar lavage samples. Ann. Clin. Lab. Sci. **22:**290–299.
86. **Collins AM, Batrawy SE, Gordon SB, Ferreira DM.** 2013. Increased IgG but normal IgA anti-pneumococcal protein antibodies in lung of HIV-infected adults. Vaccine **31:**3469–3472. http://dx.doi.org/10.1016/j.vaccine.2013.04.062.